Developmental Cell

Volume 57
Number 12
June 20, 2022

CellPress

Article

Developmental Cell

A cilia-independent function of BBSome mediated by DLK-MAPK signaling in *C. elegans* photosensation

Graphical abstract

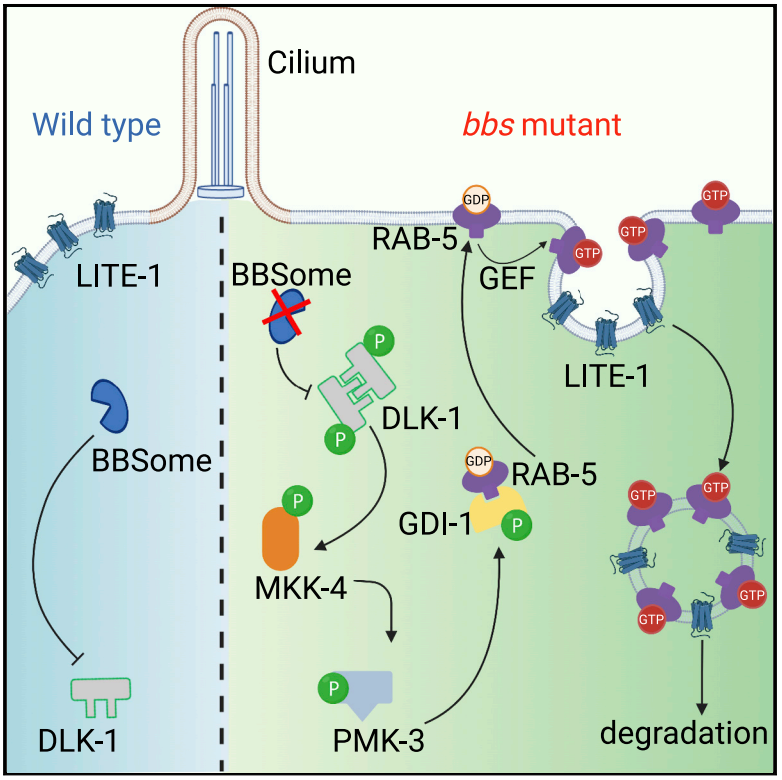

Highlights

- A genetic screen identifies BBSome as a regulator of *C. elegans* photoreceptor LITE-1
- BBSome, a ciliary protein complex, regulates LITE-1 stability independently of cilia
- BBSome regulation of LITE-1 is mediated by DLK-MAPK signaling
- BBSome inhibits the expression of DLK in both worms and human cells

Authors

Xinxing Zhang, Jinzhi Liu, Tong Pan, Alex Ward, Jianfeng Liu, X.Z. Shawn Xu

Correspondence

shawnxu@umich.edu

In brief

The BBSome complex is best known for its role in maintaining the function and structure of cilia. Zhang, Liu et al. report a cilia-independent role for the BBSome. They show that the BBSome regulates the stability of the *C. elegans* photoreceptor protein LITE-1 through DLK-MAPK signaling.

Zhang et al., 2022, Developmental Cell *57*, 1545–1557
June 20, 2022
https://doi.org/10.1016/j.devcel.2022.05.005

CellPress

Developmental Cell

CellPress

Article

A cilia-independent function of BBSome mediated by DLK-MAPK signaling in *C. elegans* photosensation

Xinxing Zhang,[1,2,4] Jinzhi Liu,[1,2,3,4] Tong Pan,[1,2] Alex Ward,[1] Jianfeng Liu,[3] and X.Z. Shawn Xu[1,2,5,*]

[1]Life Sciences Institute, University of Michigan, Ann Arbor, MI 48109, USA

[2]Department of Molecular and Integrative Physiology, University of Michigan Medical, School, Ann Arbor, MI 48109, USA

[3]College of Life Science and Technology, Key Laboratory of Molecular Biophysics of MOE, Huazhong University of Science and Technology, Wuhan, Hubei 430074, China

[4]These authors contributed equally

[5]Lead contact

*Correspondence: shawnxu@umich.edu

https://doi.org/10.1016/j.devcel.2022.05.005

SUMMARY

Bardet-Biedl syndrome (BBS) is a genetic disorder that affects primary cilia. BBSome, a protein complex composed of eight BBS proteins, regulates the structure and function of cilia, and its malfunction causes BBS in humans. Here, we report a cilia-independent function of BBSome. To identify genes that regulate the *C. elegans* photoreceptor protein LITE-1 in ciliated ASH photosensory neurons, we performed a genetic screen and isolated *bbs* mutants. Functional analysis revealed that BBSome regulates LITE-1 protein stability independently of cilia. Through another round of genetic screening, we found that this cilia-independent function of BBSome is mediated by DLK-MAPK signaling, which acts downstream of BBSome to control LITE-1 stability via Rab5-mediated endocytosis. BBSome exerts its function by regulating the expression of DLK. BBSome also regulates the expression of LZK, a mammalian DLK in human cells. These studies identify a cilia-independent function of BBSome and uncover DLK as an evolutionarily conserved BBSome effector.

INTRODUCTION

Bardet-Biedl syndrome (BBS) is an autosomal recessive genetic disorder characterized by a wide spectrum of clinical symptoms. Retinal degeneration, obesity, polydactyly (extra fingers or toes), hypogonadism, kidney malfunction, and learning disabilities are considered the primary symptoms of BBS (Beales et al., 1999). Among these diverse symptoms, retinal degeneration associated with progressive vision loss probably represents the most common clinical feature of BBS (Beales et al., 1999). Thus far, no cure is available for BBS.

At least 21 genes are associated with BBS (Forsythe et al., 2018). Eight BBS proteins form a stable core complex termed BBSome (Loktev et al., 2008; Nachury et al., 2007). BBSome is important for maintaining the function of cilia and, to a lesser extent, the structure of cilia (Ansley et al., 2003; Jin et al., 2010; Loktev et al., 2008; Nachury et al., 2007). For example, BBSome facilitates the transport of cargo proteins into cilia and is also required for retrieving signaling molecules from cilia (Berbari et al., 2008; Jin et al., 2010; Nager et al., 2017; Seo et al., 2009; Tadenev et al., 2011; Ye et al., 2018; Zhang et al., 2013). BBSome has been shown to be associated with intraflagellar transport (IFT) and undergoes bidirectional movement along cilia in mammalian neurons (Williams et al., 2014). Thus, BBSome maintains the proper function of cilia mainly by regulating protein trafficking both in and out of cilia, and BBS has accordingly been classified as a cilia disease (ciliopathy). However, how ciliary dysfunctions of BBSome may lead to BBS in patients remains unclear. Further, given the pleiotropic nature of BBS symptoms, the question arises as to whether all BBS symptoms result from ciliary dysfunctions.

The nematode *Caenorhabditis elegans* represents a highly valuable genetic model organism for the study of BBS (Bae and Barr, 2008; Inglis et al., 2007). Eight highly conserved *bbs* genes are found in the *C. elegans* genome (Bae and Barr, 2008; Inglis et al., 2007). Among them, seven encode BBSome components, and the other one encodes a homolog of the human GTPase BBS3/Arl6, ARL-6 (Bae and Barr, 2008; Inglis et al., 2007). All worm *bbs* genes are exclusively expressed in ciliated neurons under the control of the transcription factor DAF-19 (Ansley et al., 2003; Fan et al., 2004; Inglis et al., 2007). In these neurons, BBSome is localized throughout cilia (Li et al., 2004; Wei et al., 2012), and disruption of BBSome results in slightly truncated cilia (Blacque et al., 2004). Similar to mammalian BBSome, the worm BBSome directly interacts with IFT subcomplexes, coordinates IFT complex movement, and is essential for IFT complex assembly (Blacque et al., 2004; Ou et al., 2005; Wei et al., 2012). Mutations in worm *bbs* genes cause pleiotropic phenotypes, some of which are reminiscent of those observed in BBS human patients, such as obesity and learning disabilities

(Lee et al., 2011; Mak et al., 2006; Torayama et al., 2007). BBSome mutant worms also display moderate sensory defects at the behavioral level (Blacque et al., 2004; Tan et al., 2007) and show increased dense-core vesicle secretion, a phenotype that can be suppressed without affecting cilia deficits (Lee et al., 2011). Nevertheless, the precise functions of BBSome in *C. elegans* and its relationship with cilia are incompletely understood.

Here, we report a cilia-independent function of BBSome in *C. elegans*. In a screen for genes regulating the photoreceptor protein LITE-1 in ciliated ASH photosensory neurons, we isolated several *bbs* mutants. Further analysis showed that BBSome regulates the stability of LITE-1 protein in ASH neurons in a cilia-independent manner. Interestingly, LITE-1 is a nonciliary protein in ASH neurons, and BBSome can act outside of cilia to regulate LITE-1. To obtain further insights into how BBSome regulates LITE-1, we conducted another round of genetic screening for mutants suppressing the *bbs* mutant phenotype and identified *dlk-1* as a suppressor. We found that BBSome regulates LITE-1 via DLK-MAPK signaling that promotes LITE-1 protein instability via the Rab5-mediated endocytosis pathway. We further showed that BBSome acts by regulating the expression levels of DLK-1 in ASH neurons. Remarkably, BBSome also regulates the expression of LZK, a mammalian DLK in human cells. Thus, BBSome may exert its function outside of cilia via DLK-MAPK signaling. This identifies a cilia-independent BBSome function and uncovers DLK as an evolutionarily conserved effector of BBSome. Our study also raises the possibility that some of the pleiotropic symptoms of BBS in human patients might result from cilia-independent actions of BBSome.

RESULTS

BBSome is required for ASH neurons to sense light

Despite their lack of eyes, worms are sensitive to short-wavelength light and engage in negative phototaxis behavior to avoid light (Ward et al., 2008). Worms sense light through the photoreceptor protein LITE-1, a unique type of light sensor (Edwards et al., 2008; Gong et al., 2016; Liu et al., 2010). A group of ciliated sensory neurons (e.g., ASH, ASK, ASJ, AWB, etc.) are required for light-evoked avoidance response in the head region (Ward et al., 2008). Among them, ASH is somewhat special in that it is a polymodal nociceptive neuron, sensing nearly all types of aversive cues, including odorants, tastants, mechanical forces, high osmolarity, pH, etc. (Bargmann, 2006; Wang et al., 2016). While the photosensation mechanisms in some photoreceptor neurons such as ASK and ASJ have been well characterized (Liu et al., 2010), little is known about how ASH neurons sense light. To address this question, we first confirmed that ASH neurons are light sensitive and found that, as reported (Zhang et al., 2020), light evoked a robust calcium response in these neurons (Figures 1A and 1B). ASH photosensitivity was not altered in *unc-13* and *unc-31* mutants, which are defective in secreting small neurotransmitters and neuropeptides, respectively (Richmond et al., 1999; Speese et al., 2007), indicating that the observed light response in ASH neurons primarily arose from ASH neurons cell autonomously (Figures 1A and 1B). As expected (Zhang et al., 2020), LITE-1 is required for ASH neurons to sense light, as the *lite-1(xu492)* mutant, a deletion allele of *lite-1*, did not respond to light stimulation (Figures 1A and 1B).

We then designed a forward genetic screen to identify genes that regulate ASH photosensitivity. We labeled ASH neurons with a genetically encoded calcium indicator (GECI) that emits fluorescence when excited by blue light (Figure 1C). As ASH neurons show sensitivity to blue light, we were able to detect an increase in fluorescence intensity in ASH neurons upon light stimulation (Figure 1C). Taking advantage of this observation, we mutagenized worms with EMS and visually screened for mutants that failed to exhibit light-evoked increase in fluorescence intensity (Figure S1A). After going through ~36,000 F2 worms (from ~2,000 F1), we isolated 14 mutants. Among them, two (i.e., *xu580[S320F]* and *xu592[P112L]*) are *lite-1* alleles, validating the screen. Interestingly, we isolated five mutants that were mapped to *bbs* genes, including *bbs-1*, *bbs-7*, *bbs-8*, and *bbs-9* (Figures 1D and S2A–S2C). To verify the phenotype, we examined deletion alleles of these *bbs* genes and observed a similar phenotype (Figures 1E–1M). Since we hit half of the genes that encode protein products of the *C. elegans* BBSome, we wondered whether all the *bbs* genes are required for ASH neurons to sense light. Remarkably, seven out of eight BBSome genes are essential for ASH neurons to respond to light (Figures 1E–1M). Loss of *arl-6*, the remaining BBSome-associated gene that encodes a homolog of human GTPase BBS3/Arl6, also led to a defect in ASH photosensitivity (Figures 1G and 1M). Thus, it appears that all BBSome components are important for ASH neurons to sense light.

A specific role of BBSome in regulating photosensation in ASH neurons

Since ASH neurons are polymodal sensory neurons, we asked whether BBSome is important for ASH neurons to sense other sensory cues, such as high osmolarity (glycerol), heavy metals (copper), and detergents (SDS). We focused on BBS-1 and BBS-8, two core components of BBSome. Both *bbs-1* and *bbs-8* mutants responded robustly to all tested stimuli (Figures S3A–S3F). As a control, *osm-9* mutant worms exhibited a severe defect (Figures S3A–S3F). We also found that although ASH neurons lost photosensitivity in *bbs* mutants, ASK neurons responded normally to light in these mutants (Figures S3G and S3H). The ASH photo-insensitivity phenotype in *bbs* mutants was rescued by transgenic expression of wild-type (WT) *bbs* genes in ASH neurons, indicating that BBSome acts in ASH neurons to regulate their photosensitivity (Figures S3I and S3J). At the behavioral level, *bbs-1* and *bbs-8* mutants displayed a mild defect (Figure S4A), likely due to the presence of other photosensory neurons such as ASK and ASJ. Indeed, genetic ablation of these neurons with a caspase then resulted in a more severe defect in phototaxis (Figure 1N). These data together reveal a specific role for BBSome in regulating photosensation in ASH neurons.

Cilia are not required for ASH to sense light

In *C. elegans*, BBSome is required for intraflagellar transport (IFT), which is important for building and maintaining the structure and function of cilia (Bae and Barr, 2008; Inglis et al., 2007). The observation that *bbs* mutants lacked photosensitivity in ASH neurons suggests that cilia are essential for ASH neurons

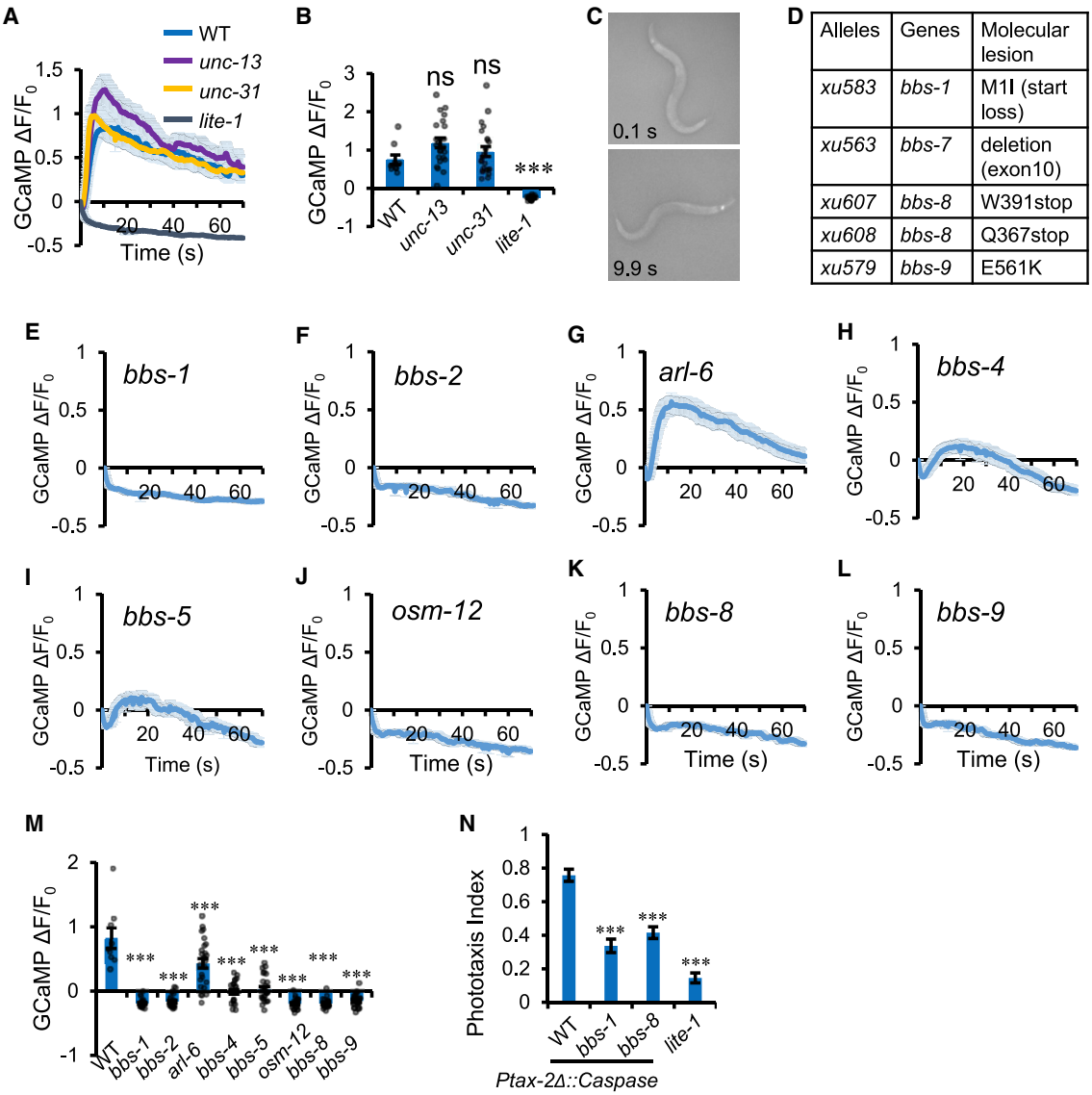

Alleles	Genes	Molecular lesion
xu583	*bbs-1*	M1I (start loss)
xu563	*bbs-7*	deletion (exon10)
xu607	*bbs-8*	W391stop
xu608	*bbs-8*	Q367stop
xu579	*bbs-9*	E561K

Figure 1. *bbs* genes are required for ASH neurons to sense light

(A) ASH neurons sense light cell autonomously in a LITE-1-dependent manner. Calcium imaging was performed on WT, *unc-13(e51)*, *unc-31(e169)*, and *lite-1(xu492)* worms. GCaMP6f was expressed as a transgene in ASH neurons using the *sra-6* promoter. Worms were imaged and stimulated with blue light. Shown are calcium traces. Shades along the traces denote error bars (SEM).

(B) Bar graph summarizing the data in (A). Error bars: SEM; n ≥ 9; ***p < 0.0001; ns: not significant; ANOVA with Bonferroni test.

(C) Snapshot images. Upon blue light illumination, the fluorescence in ASH neurons in a moving worm turned brighter, enabling a genetic screen for mutants insensitive to light stimulation. The strain carried a transgene expressing the genetically encoded calcium sensor Case12 in ASH neurons under the *sra-6* promoter.

(D) Five mutant alleles identified from the genetic screen were mapped to *bbs* genes, including *bbs-1(xu583), bbs-7(xu563), bbs-8(xu607), bbs-8(xu608)*, and *bbs-9(xu579)*.

(E–L) Calcium imaging of *bbs-1(ok1111)*, *bbs-2(ok2053)*, *arl-6/bbs-3(ok3472)*, *bbs-4(tm3038)*, *bbs-5(gk537)*, *osm-12/bbs-7(ok1351)*, *bbs-8(nx77)*, and *bbs-9(gk471)* mutant worms. All strains carried the same GCaMP transgene. Shown are calcium imaging traces. Shades along each trace denote error bars (SEM).

(M) Bar graph summarizing the data in (E–L). Error bars: SEM; n ≥ 9; ***p < 0.0001; ANOVA with Bonferroni test.

(N) Phototaxis assay shows that *bbs-1(ok1111)* and *bbs-8(nx77)* are defective at the behavior level in *Ptax-2Δ::Caspase* background, in which other photosensory neurons (e.g., ASK, AWB, and ASJ) are genetically ablated. Error bars: SEM. n ≥ 22; ***p < 0.0001; ANOVA with Bonferroni test.

See also Figures S1–S3.

to sense light. To test this idea, we examined cilia-defective mutants, particularly those affecting IFT, such as *osm-3* (kinesin motor), *che-3* (dynein motor), *daf-10* (IFT-A component), *osm-5* (IFT-B component), *klp-11* (kinesin-II motor), and *kap-1* (kinesin-associated protein) (Figures 2A and 2B). In our genetic screen, we excluded mutants with severe defects in ASH morphology, which may explain the fact that we did not recover these cilia-defective mutants. Here, we found that while

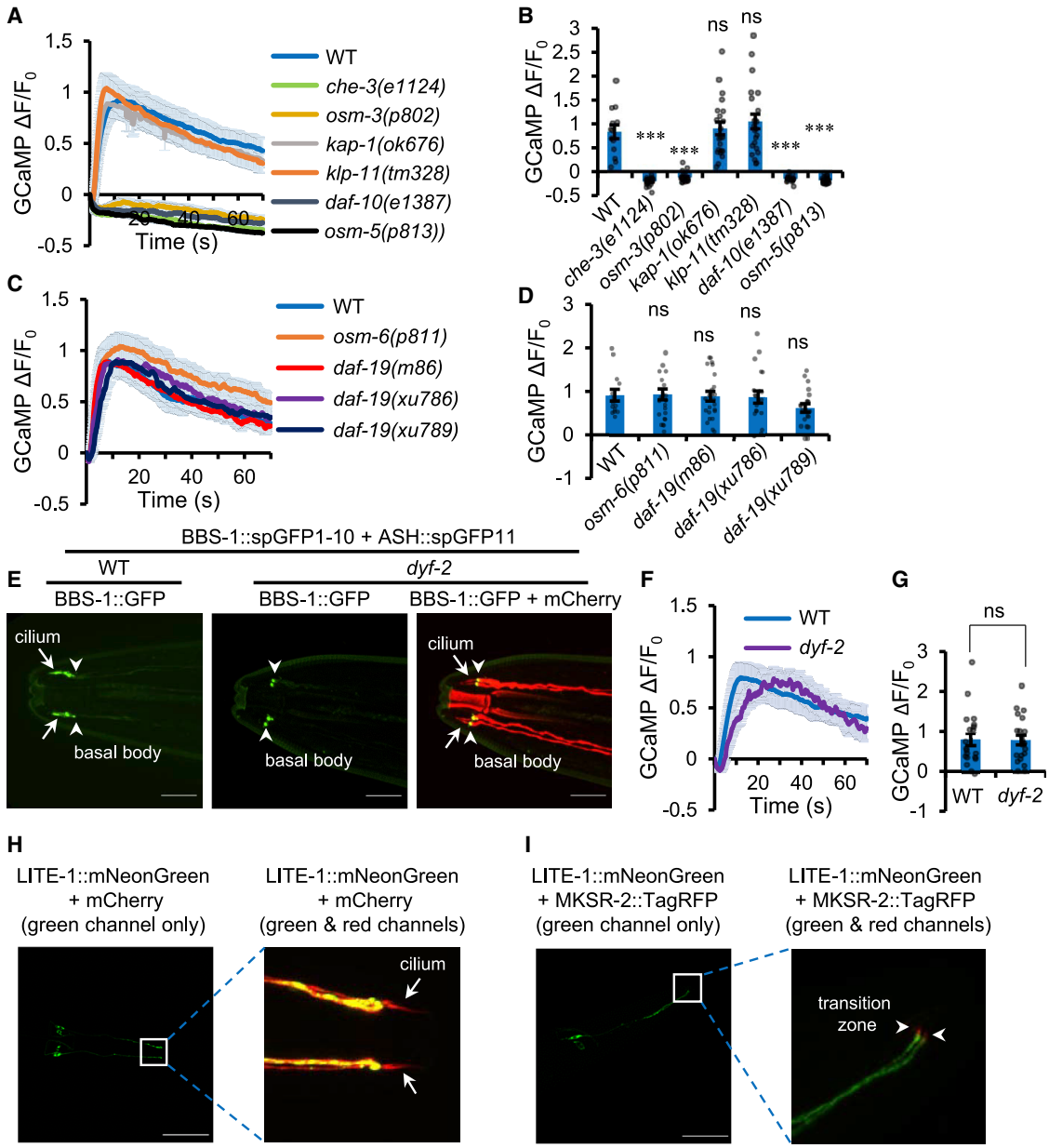

Figure 2. Cilia are not required for ASH neurons to sense light and LITE-1 is a nonciliary protein in ASH neurons

(A and B) Not all IFT mutants are defective in photosensation in ASH neurons. All strains carried the same GCaMP transgene.

(A) Calcium imaging traces with shades along the traces denoting error bars (SEM).

(B) Bar graph. Error bars: SEM; n ≥ 13; ***p < 0.0001;. ns: not significant; ANOVA with Bonferroni test.

(C and D) *osm-6* and *daf-19* mutant worms respond normally to light in ASH neurons. All worms carried the same GCaMP transgene. As *daf-19* mutants form dauers, all *daf-19* strains were in the *daf-12(sa204)* mutant background. *xu786* and *xu789* are deletion alleles of *daf-19* generated by CRISPR-Cas9-based genome editing.

(C) Calcium imaging traces. The shades along the traces denote error bars (SEM).

(D) Bar graph. Error bars: SEM; n ≥ 14.

(E) BBSome is enriched in cilia in WT but excluded from cilia in *dyf-2(jhu616)* mutant. BBSome was marked by BBS-1::GFP fluorescence. Endogenous BBS-1 was fused with a C terminus spGFP1-10 tag by CRISPR-Cas9-mediated genome editing and visualized in ASH by expressing a transgene *Psra-6::7xspGFP11* that drove expression of a 7× spGFP11 fragment in ASH neurons to reconstitute BBS-1::GFP. ASH cilia in *dyf-2(jhu616)* were visualized using the transgene *Psra-6::mCherry*. Shown are confocal images. Left: green channel showing BBS-1::GFP in WT; middle: green channel showing BBS-1::GFP in *dyf-2(jhu616)* mutant; right: merged green and red channels showing BBS-1::GFP and ASH::mCherry in *dyf-2(jhu616)* mutant, which demonstrates that cilia are intact in this mutant, but BBS-1 is excluded from cilia and enriched in the basal body. Arrows point to the cilium. Arrow heads point to the basal body. Scale bar: 10 μm.

(F and G) *dyf-2(jhu616)* mutant worms respond normally to light in ASH neurons. All worms carried the same GCaMP transgene.

(F) Calcium imaging traces with shades along the traces denoting error bars (SEM).

(legend continued on next page)

mutations in *osm-3, che-3, daf-10*, and *osm-5* rendered ASH neurons insensitive to light, *klp-11* and *kap-1* mutant worms showed normal response to light (Figures 2A and 2B). Thus, while some IFT components (e.g., BBSome, OSM-3, and DAF-10) are important for ASH neurons to sense light, others, such as KLP-11 and KAP-1, are not, indicating that ASH photosensitivity does not necessarily require all IFT components.

To further evaluate the role of cilia in ASH photosensitivity, we tested OSM-6, a core component of the IFT-B subcomplex (Collet et al., 1998). *osm-6* mutants are commonly used to assess ciliary functions, as their cilia are nearly eliminated (or much shortened) (Collet et al., 1998; Perkins et al., 1986). Intact ciliary structure is believed to be required for ASH neurons to sense sensory cues. In support of this notion, *osm-6(p811)* mutant worms were defective in responding to a number of aversive sensory cues, such as high osmolarity (glycerol), heavy metals (copper), and detergents (SDS) (Figures S3A–S3F). Surprisingly, ASH neurons responded normally to light in *osm-6(p811)* mutant worms (Figures 2C and 2D), suggesting that intact cilia are not required for ASH neurons to sense light.

As *osm-6(p811)* mutant worms still retain some rudimentary ciliary structure (Perkins et al., 1986), it might be argued that such defective cilia might nevertheless be sufficient to allow ASH neurons to sense light. To address this concern, we checked DAF-19, a transcription factor known to be required for the formation of cilia in all ciliated neurons. It has been reported that *daf-19(m86)* mutant worms fail to develop any type of ciliary structure, including transition zones (Perkins et al., 1986). Remarkably, *daf-19(m86)* mutant worms responded normally to light (Figures 2C and 2D). To provide further evidence, we generated two deletion alleles of *daf-19: xu786* and *xu789* by CRISPR-Cas9-based genome editing. Both *daf-19(xu786)* and *daf-19(xu789)* mutants showed normal light responses in ASH neurons (Figures 2C and 2D). Thus, we conclude that cilia are not required for ASH neurons to sense light.

Another interesting observation involves BBS-4 and BBS-5. Unlike other BBSome components, BBS-4 and BBS-5 are functionally redundant and thus not required for ciliogenesis, and both *bbs-4* and *bbs-5* mutants show normal ciliary structure (Xu et al., 2015). However, despite the presence of intact cilia in *bbs-4* and *bbs-5* mutant worms, ASH neurons in these two mutants were severely defective in responding to light (Figures 1H, 1I, and 1M). Thus, cilia are neither necessary nor sufficient for ASH neurons to sense light.

Considering that cilia are not required for ASH neurons to sense light, one would expect that BBSome would be able to act outside of cilia to regulate LITE-1 in ASH neurons. *jhu616*, a hypomorphic allele of *dyf-2* gene that encodes a key component of the IFT complex, offers an excellent opportunity to test this idea. In this strain, cilia remain intact, yet BBSome is dissociated from IFT particles (Wei et al., 2012). Consequently, BBSome is excluded from cilia and instead enriched in the basal body (Wei et al., 2012). We were able to verify this finding by showing that although cilia were intact, BBSome was indeed excluded from cilia in ASH neurons in this *dyf-2* background (Figure 2E). Despite the absence of BBSome in cilia, ASH neurons in these *dyf-2* worms responded normally to light (Figures 2F and 2G), suggesting that BBSome can act outside of cilia to regulate LITE-1.

LITE-1 is a nonciliary protein in ASH neurons

The fact that ASH neurons do not depend on cilia for photosensation raises the possibility that LITE-1 may not function in cilia. We thus checked the subcellular localization of LITE-1 protein in ASH neurons. We expressed LITE-1::mNeonGreen fusion as a transgene in ASH neurons, and mCherry was co-expressed as a marker to label the entire neuron. LITE-1::mNeonGreen fusion did not overlap with mCherry in the cilia (Figure 2H), indicating that that LITE-1 was not localized to the cilia in ASH neurons. To ascertain whether LITE-1 can enter the transition zone, we generated another transgenic strain, in which the transition zone was labeled by MKSR-2::TagRFP fusion in ASH neurons (Figure 2I). LITE-1 did not appear to overlap with MKSR-2 (Figure 2I). These data demonstrate that LITE-1 is not localized to ASH cilia or transition zone and thus identify LITE-1 as a nonciliary protein in ASH neurons. This is consistent with the observation that cilia are not required for ASH neurons to sense light.

BBSome regulates the stability of LITE-1 protein in an age-dependent manner in ASH neurons

Since LITE-1 is a nonciliary protein in ASH neurons and cilia are neither necessary nor sufficient for ASH neurons to sense light, this brings up the question of how BBSome regulates LITE-1. To assess whether and how disruption of BBSome affects LITE-1 in ASH neurons, we fused an mNeonGreen tag to the C terminus of the endogenous LITE-1 receptor by CRISPR-Cas9-based genome editing. The resulting knockin strain, named *lite-1(xu708)*, showed normal phototaxis behavior (Figure S4A), and its ASH neurons responded normally to light (Figures S4B and S4C), indicating that the mNeonGreen tag did not notably affect LITE-1 function (Figures S4A–S4C). LITE-1::mNeonGreen fluorescence was very dim, consistent with the notion that endogenous LITE-1 is expressed at a very low level (Gong et al., 2016). Notably, ASH is among those few cells in which LITE-1 was expressed at a relatively higher level, making it possible to visually identify this neuron in the knockin strain (Figure 3A). Again, we focused on characterizing BBS-1 and BBS-8, two core components of BBSome. At the larval stages

(G) Bar graph. Error bars: SEM; n $\geq$ 20; ns: not significant; t test.

(H) LITE-1 is not localized to ASH cilia. Shown are confocal images of transgenic worms, in which LITE-1::mNeonGreen (LITE-1::mNG) fusion protein was expressed in ASH neurons together with mCherry under the *sra-6* promoter. For convenience, only the green channel was shown in the image in the left panel. Shown on the right is a zoomed-in image with both the green and red channels. Arrows point to the cilium where LITE-1::mNeonGreen signals (green) are absent. Scale bar: 50 μm.

(I) LITE-1 is not localized to the transition zone in ASH. Shown are confocal images of transgenic worms, in which LITE-1::mNeonGreen fusion protein was expressed in ASH neurons together with MKSR-2::TagRFP fusion protein under the *sra-6* promoter. For convenience, only the green channel was shown in the image in the left panel. Shown on the right is a zoomed-in image with both the green and red channels. MKSR-2 is a transition zone marker. Arrow heads point to the transition zone (red) where LITE-1::mNeonGreen (green) signals are absent. Scale bar: 50 μm.

See also Figure S4.

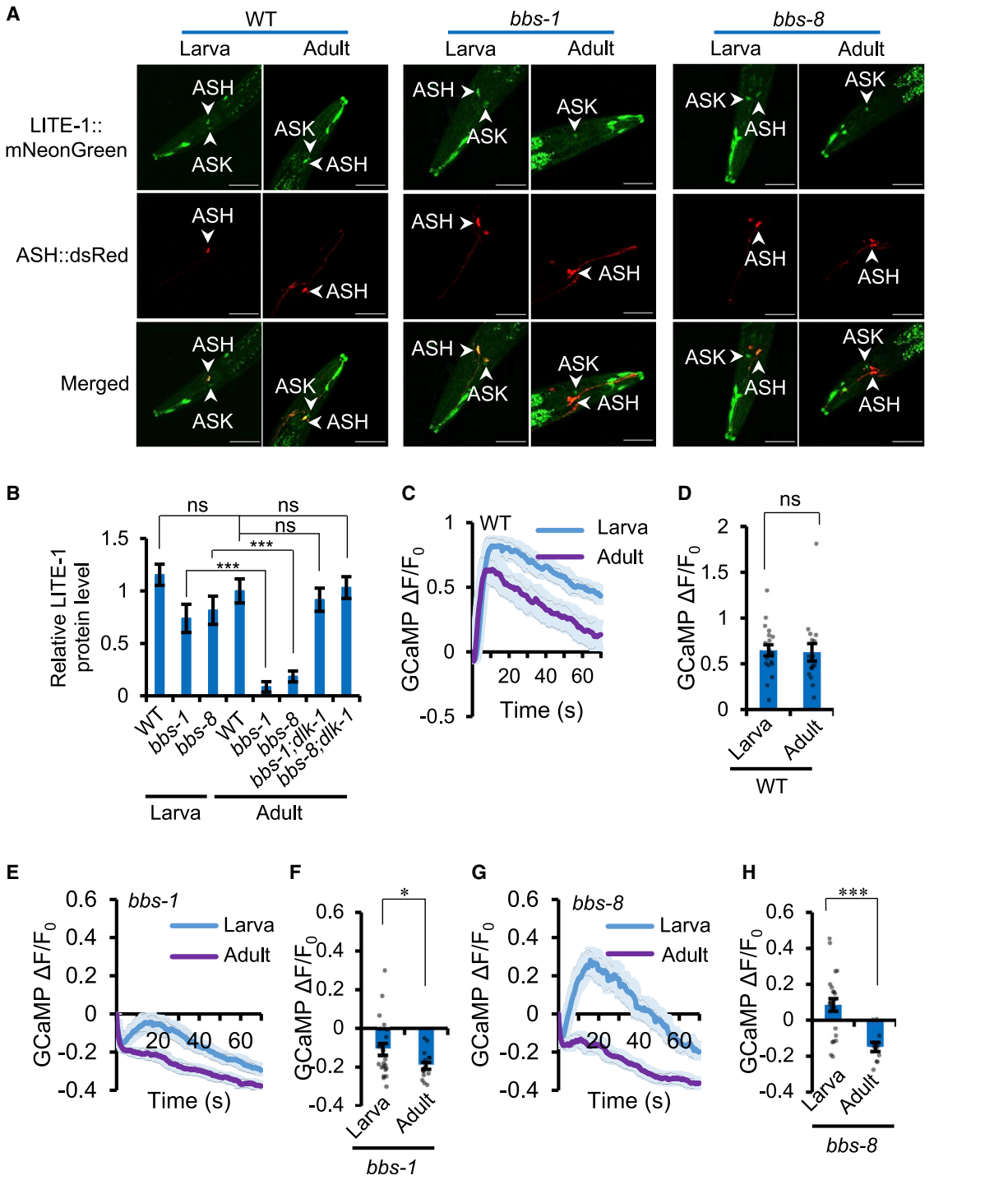

Figure 3. Progressive loss of LITE-1 protein in ASH neurons of *bbs* mutants in an age-dependent manner

(A) LITE-1 protein is present at the larval stage but absent at the adult stage in *bbs* mutant worms. Shown are confocal images for *lite-1(xu708[LITE-1::mNeonGreen])*; *xuEx[Psra-6::dsRed]* in WT, *bbs-1(ok1111)*, and *bbs-8(nx77)* genetic backgrounds at both the larval (L4) and adult (day 2) stages. *lite-1(xu708[LITE-1::mNeonGreen])* is a CRISPR-Cas9 knockin strain, in which an mNeonGreen tag was fused to the C terminus of LITE-1. *xuEx[Psra-6::dsRed]* was used to label ASH neurons. LITE-1 protein was found in both ASH and ASK neurons in WT worms at both the larval and adult stages. However, in *bbs* mutants, LITE-1 in ASH neurons can only be detected at the larval stage, but not at the adult stage. Scale bar: 50 μm.

(B) Bar graph quantifying the data in (A) and Figure 4D. Error bars: SEM; n ≥ 23;.

***p < 0.0001; t test.

(C and D) ASH neurons in WT worms at both the larva and adult stages respond to light.

(legend continued on next page)

up to L4, we detected LITE-1 protein in ASH neurons of *bbs* mutant and WT worms (Figures 3A and 3B). However, at the adult stage beginning at day 2, we could no longer detect LITE-1 protein in ASH neurons of *bbs* mutants, although LITE-1 expression in ASH neurons persisted in WT worms (Figures 3A and 3B). This was not due to the loss of ASH neurons in adult *bbs* mutant worms, as ASH neurons were clearly present in the mutants and also responded normally to other aversive sensory cues (Figures 3A and S3A–S3F). The length of ASH cilia in adult *bbs* mutant worms also appeared normal (Figure S4D). As an internal control, we found that LITE-1 expression was normal in ASK neurons of *bbs* mutants at both the larval and adult stages (Figure 3A). Thus, mutations in *bbs* genes cause an age-dependent loss of LITE-1 expression in ASH neurons.

We then assayed the *lite-1* mRNA levels in *bbs* mutants. To do so, we first isolated ASH neurons by fluorescence-activated cell sorting (FACS) (Kaletsky et al., 2016) and then extracted their RNA. qRT-PCR analysis detected no significant difference in the *lite-1* mRNA levels between WT and *bbs* mutants in adult worms (Figure S4E), indicating that *bbs* mutations do not affect the mRNA levels of *lite-1*. This suggests that BBSome is important for maintaining the stability of LITE-1 protein in ASH neurons. Consistent with this notion, at the functional level, ASH neurons indeed responded to light in *bbs* mutants at the larval stage, although the amplitude of the response was reduced; by constrast, no such light response was detected in adult worms of these mutants (Figures 3C–3H). These results together unveil an important role for BBSome in regulating the stability of LITE-1 protein in ASH neurons in an age-dependent manner.

A suppressor screen reveals that DLK-1 acts downstream of BBSome to regulate LITE-1 stability in ASH neurons

To obtain insights into how BBSome regulates LITE-1, we performed a suppressor screen for mutants that suppressed the photo-insensitive phenotype associated with *bbs* mutant worms. To do so, we screened for mutant worms that regained sensitivity to light in ASH neurons of *bbs-8* mutant worms (Figure S1B). After screening ~40,000 F2 worms (from ~2,000 F1), we isolated 15 suppressors. We focused on three such suppressors, *xu734, xu735*, and *xu736*, that displayed a strong suppression effect on the *bbs* mutant phenotype. By whole-genome sequencing, we found that they are mutants of the *dlk-1* gene (Figure S2D). As all these three *dlk-1* alleles harbor missense mutations and are likely hypomorphs (Figure 4A), we tested a null allele of *dlk-1*. Though *dlk-1* null mutation did not notably affect ASH photosensitivity (Figures S5A and S5B), it can restore photosensitivity in ASH neurons of *bbs-1* and *bbs-8* mutant worms (Figures 4B and 4C). This suppression effect was rescued by transgenic expression of the WT *dlk-1* gene in ASH neurons (Figures 4B and 4C), demonstrating that *dlk-1* acts in ASH to suppress the phenotype of *bbs* mutant worms. These data suggest that DLK-1 acts downstream of BBSome to regulate LITE-1 in ASH neurons. In support of this, loss of *dlk-1* also suppressed the LITE-1 protein instability phenotype in *bbs* mutant worms (Figures 4D and 3B); specifically, LITE-1 protein can now be detected in ASH neurons in *bbs* adult mutant worms (Figures 4D and 3B). We thus conclude that DLK-1 acts downstream of BBSome to regulate LITE-1 stability in ASH neurons.

DLK/p38MAPK signaling acts downstream of BBSome to regulate LITE-1 in ASH neurons

DLK-1 is the *C. elegans* orthologue of the dual leucine zipper kinase (DLK) MAPKKK, which functions in a p38MAPK signaling cascade consisting of DLK-1/MAPKKK, MKK-4/MAPKK, and the PMK-3 p38MAPK (Jin and Zheng, 2019). This DLK/p38MAPK signaling is known to regulate synaptogenesis, axon growth, and axon regeneration (Jin and Zheng, 2019), but has not been implicated in BBSome functions. To garner additional evidence, we tested the potential involvement of MKK-4/MAPPK and PMK-3/MAPK in suppressing *bbs* mutant phenotype. Similar to the case with *dlk-1*, although mutations in *mkk-4* and *pmk-3* did not notably affect ASH photosensitivity, they suppressed the photo-insensitive phenotype observed in ASH neurons of *bbs-1* and *bbs-8* mutant worms (Figures S5A, S5B, and 5A–5D). This suggests that the DLK/p38MAPK signaling cascade acts downstream of BBSome to regulate LITE-1 in ASH neurons.

DLK/p38MAPK signaling regulates LITE-1 protein stability through Rab5-mediated endocytosis pathway

We wondered how DLK/p38MAPK signaling regulates LITE-1 protein stability. In addition to synaptogenesis, axon growth, and axon regeneration, DLK/p38MAPK signaling has also been reported to promote the endocytosis of membrane receptors to downregulate their expression (Park et al., 2009). Specifically, p38MAPK can stimulate Rab5-mediated endocytosis by phosphorylating and activating the GDP dissociation inhibitor (GDI) of Rab5 (Cavalli et al., 2001). As a first step to test the role of Rab5, we generated a transgenic line expressing *rab-5(CA)*, a constitutively active, gain-of-function form of the worm Rab5 homolog RAB-5, in ASH neurons (Sann et al., 2012). The *rab-5(CA)* transgene suppressed the photosensitivity of ASH neurons in WT worms, as well as *bbs-1; dlk-1*

(C) ASH calcium imaging traces from worms at the larva (L4) and adult (day 1) stages. Shades along the traces denote error bars (SEM).
(D) Bar graph. Error bars: SEM; n ≥ 16; ns: not significant (t test).
(E and F) ASH neurons in *bbs-1* mutant worms at the larval stage show weak responses to light, but those at the adult stage do not.
(E) Calcium imaging traces from *bbs-1(ok1111)* mutant worms at the larval (L4) and adult (day1) stages. Shades along the traces denote error bars (SEM). Some readings became negative due to the basal line drift likely caused by GCaMP fluorescence photobleaching over time.
(F) Bar graph. Error bars: SEM. n ≥ 16; *p < 0.05; t test.
(G and H) ASH neurons in *bbs-8* mutant worms at the larval stage show weak responses to light, but those at the adult stage do not.
(G) Calcium imaging traces from *bbs-8(nx77)* mutant worms at the larval (L4) and adult (day1) stages. Shades along the traces denote error bars (SEM). Some readings became negative due to the basal line drift likely caused by GCaMP fluorescence photobleaching over time.
(H) Bar graph. Error bars: SEM; n ≥ 12; ***p < 0.0001; t test.
See also Figure S4.

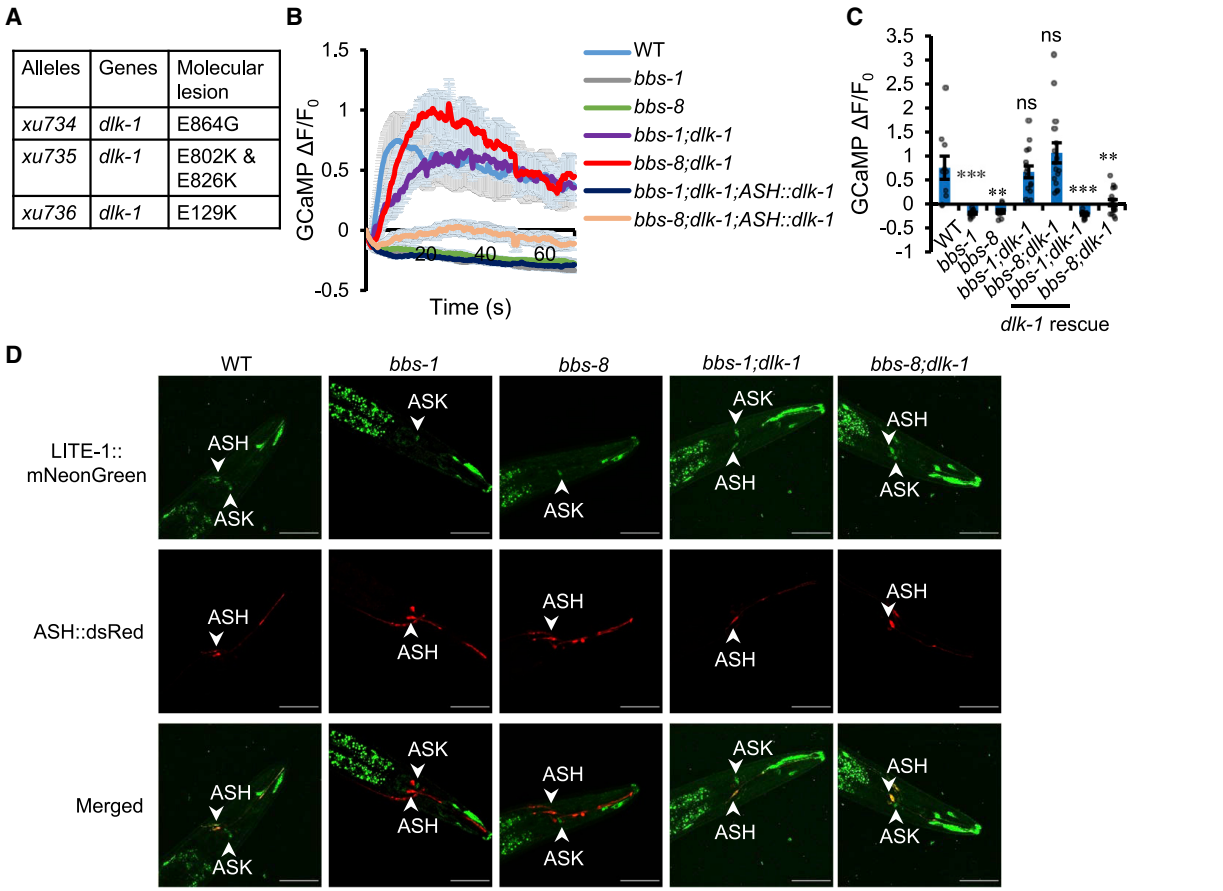

Figure 4. DLK-1 acts downstream of BBSome to regulate LITE-1 in ASH neurons

(A) Three mutant alleles identified from the suppressor screen are mapped to *dlk-1*, including *dlk-1(xu734)*, *dlk-1(xu735)*, and *dlk-1(xu736)*.

(B and C) Loss of *dlk-1(km12)* suppresses the photo-insensitivity phenotype of *bbs-1* and *bbs-8* mutants. ASH neurons in *bbs-1;dlk-1* and*bbs-8;dlk-1* double-mutant worms became sensitive to light, while *bbs-1* and *bbs-8* single mutant worms were not. This phenotype was rescued by transgenic expression of *dlk-1* cDNA in ASH neurons under the *sra-6* promoter.

(B) Calcium imaging traces. Shades along the traces denote error bars (SEM).

(C) Bar graph. Error bars: SEM; n ≥ 10; ***p < 0.0001; ** p < 0.005, ns: not significant; ANOVA with Bonferroni test.

(D) Loss of *dlk-1(km12)* suppresses the LITE-1 protein instability phenotype of *bbs* mutant worms. Shown are confocal images for *lite-1(xu708[LITE-1::mNeonGreen]);xuEx[Psra-6::dsRed]* in WT, *bbs-1*, *bbs-8, dlk-1;bbs-1*, and *dlk-1;bbs-8* genetic backgrounds at adult (day 2) stage. *xuEx[Psra-6::dsRed]* was used to label ASH neurons. LITE-1 protein was lost in ASH neurons of *bbs-1* and *bbs-8* mutant worms but can be detected in *bbs-1;dlk-1* and *bbs-8;dlk-1* double-mutant worms. Scale bar, 50 μm.

See also Figures S1, S2, and S5.

and *bbs-8; dlk-1* worms (Figures 6A and 6B), which is consistent with the notion that RAB-5 acts downstream of DLK/p38MAPK signaling to regulate LITE-1. We then sought to test the effect of *rab-5* loss-of-function on LITE-1. As both *rab-5* and *gdi-1* are required for viability, we were unable to test their mutants. We therefore examined RABX-5 and RME-6, the GEFs that are required for the function of RAB-5 (Sann et al., 2012; van der Vaart et al., 2015). Loss of these two Rab5 GEFs inhibits Rab5-mediated endocytosis (Sann et al., 2012; Sato et al., 2005). We found that mutations in these two RAB-5 GEFs suppressed the ASH photo-insensitive phenotype of *bbs* mutants (Figures 6C–6F). Loss of *rabx-5* and *rme-6* also suppressed the LITE-1 protein instability phenotype observed in *bbs* mutants (Figure S6). These findings together suggest that DLK/p38MAPK signaling regulates LITE-1 stability via Rab5-mediated endocytosis pathway.

BBSome regulates the expression levels of DLK-1

Having characterized how DLK-1 regulates LITE-1, we then asked how DLK-1 is regulated by BBSome. As DLK/MAPKKKs are self-activated by homomultimerization and auto-phosphorylation, a common strategy to regulate these MAPKKKs is to modulate their expression levels (Jin and Zheng, 2019). RPM-1, an E3 ubiquitin ligase, is the best-known DLK regulator, which negatively regulates DLK-1 by promoting its protein degradation (Nakata et al., 2005; Yan et al., 2009). We tested RPM-1 but found that *rpm-1* mutants did not have a phenotype in ASH photosensitivity (Figures S5A and S5B). Overexpression of *rpm-1* in ASH also exhibited no notable phenotype (Figures S5C and S5D). We thus wondered if the mRNA level of DLK-1 is regulated by BBSome. To test this, we purified ASH neurons from WT and *bbs* mutant worms by FACS and extracted their RNA. qRT-PCR analysis showed that the *dlk-1* mRNA level

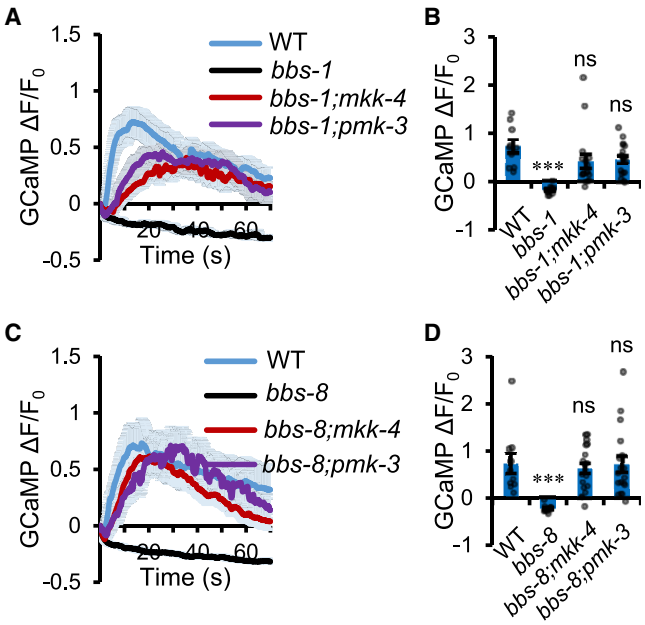

Figure 5. DLK-1/p38MAPK signaling acts downstream of BBSome to regulate LITE-1 in ASH neurons

(A and B) Loss of *mkk-4*/MAPKK and *pmk-3*/p38 MAPK suppresses the photoinsensitive phenotype of *bbs-1* mutant worms. ASH neurons in *bbs-1;mkk-4* and *bbs-1;pmk-3* double-mutant worms became sensitive to light, while *bbs-1* single mutant worms were not.

(A) Calcium imaging traces. Shades along the traces denote error bars (SEM).

(B) Bar graph. Error bars: SEM; n ≥ 10; ***p < 0.0001; ANOVA with Bonferroni test.

(C and D) Loss of *mkk-4*/MAPKK and *pmk-3*/p38 MAPK suppresses the photoinsensitive phenotype of *bbs-8* mutant worms. ASH neurons in *bbs-8;mkk-4* and *bbs-8;pmk-3* double-mutant worms became sensitive to light, while *bbs-8* single-mutant worms were not.

(C) Calcium imaging traces. Shades along the traces denote error bars (SEM).

(D) Bar graph. Error bars: SEM; n ≥ 10; ***p < 0.0001; ANOVA with Bonferroni test.

See also Figure S5.

was elevated in *bbs-1* and *bbs-8* mutant worms (Figure 7A). To assess whether the protein level of DLK-1 is also upregulated in *bbs* mutants, we inserted an mNeonGreen tag into the endogenous *dlk-1* gene by CRISPR-Cas9-mediated genome editing. We observed an increase in mNeonGreen::DLK-1 fluorescence in *bbs-1* and *bbs-8* mutant worms (Figure S7), indicating that the DLK-1 protein level was also upregulated in *bbs* mutants. Thus, BBSome appears to negatively regulate the expression of DLK-1. This points to a model whereby BBSome promotes LITE-1 protein stability by negatively regulating DLK-1 (Figure 7F).

If BBSome promotes LITE-1 stability by negatively regulating DLK-1, then upregulating DLK-1 expression in ASH neurons should be sufficient to inhibit LITE-1 expression and hence its function. To test this, we overexpressed DLK-1 as a transgene in ASH neurons and found that DLK-1 overexpression strongly suppressed the photosensitivity of ASH neurons (Figures 7B and 7C), a phenotype reminiscent of that observed in *bbs* mutants. In addition, DLK-1 overexpression led to a strong reduction in LITE-1 protein levels in ASH neurons (Figures 7D and 7E), a phenotype similar to that observed in *bbs* mutants (Figures 3A and 3B). Thus, DLK-1 appears to inhibit LITE-1 expression and hence its function in ASH neurons. These data lend further support to the model that BBSome promotes LITE-1 protein stability by negatively regulating DLK/p38MAPK signaling (Figure 7F). These results identify DLK-1 as an effector of BBSome.

BBSome regulates the expression levels of the human DLK-1 homolog LZK

As both BBSome and DLK/MAPKKK are evolutionarily conserved, this prompted us to ask whether BBSome plays a similar role in mammals by negatively regulating DLK/MAPKKK expression. To test this, we knocked down the human BBS-1 and BBS-8 homologs BBS1 and BBS8/TTC8, respectively, in HeLa cells, and then examined the mRNA levels of two human DLK-1 homologs: LZK and DLK. qRT-PCR analysis showed that siRNA knockdown of BBS1 and BBS8/TTC8 in HeLa cells potentiated the mRNA levels of LZK in these cells (Figure 7G). This suggests that BBSome may play an evolutionarily conserved role by negatively regulating DLK/MAPKKK in both worm and human cells.

DISCUSSION

A cilia-independent function of BBSome in regulating protein stability

BBSome is best known for its role in maintaining the function and structure of cilia. BBS has thus been classified as ciliopathy, a disorder caused by ciliary dysfunctions (Beales et al., 1999). In addition, BBS manifests a wide range of clinical symptoms, such as retinal degeneration, obesity, polydactyly, hypogonadism, kidney malfunction, and learning disabilities (Beales et al., 1999). Such diverse symptoms raise the question as to whether all the BBS symptoms arise from ciliary dysfunctions (Novas et al., 2015); however, it remains a challenge to test this. Here, through an unbiased genetic screen and the use of cilia-absent mutants (e.g., *daf-19*), we identified a cilia-independent function of BBSome in regulating the stability of the photoreceptor protein LITE-1 in *C. elegans*. Characterization of a *dyf-2* mutant, in which cilia remain intact but BBSome is excluded from cilia, further suggests that BBSome can act outside of cilia to regulate LITE-1. Our results provide direct evidence that BBSome can function independently of cilia.

Interestingly, a recent report showed that the ciliary protein ARL13B can regulate Sonic hedgehog (Shh) signaling outside of cilia in mice (Gigante et al., 2020). Although the underlying mechanisms are unclear, the ciliary and extra-ciliary roles of ARL13B can be uncoupled. Thus, the function of ciliary proteins may not be restricted to cilia, and these proteins may possess extra-ciliary roles, a phenomenon that may be more common than currently recognized.

One interesting observation is that BBSome regulates the stability of the photoreceptor protein LITE-1 in an age-dependent manner. In *bbs* mutant worms, ASH photosensory neurons progressively lose LITE-1 protein and hence their photosensitivity in an age-dependent manner. Though BBS displays pleiotropic symptoms, vision loss represents the most common clinical symptom of BBS patients. Strikingly, the vision loss suffered

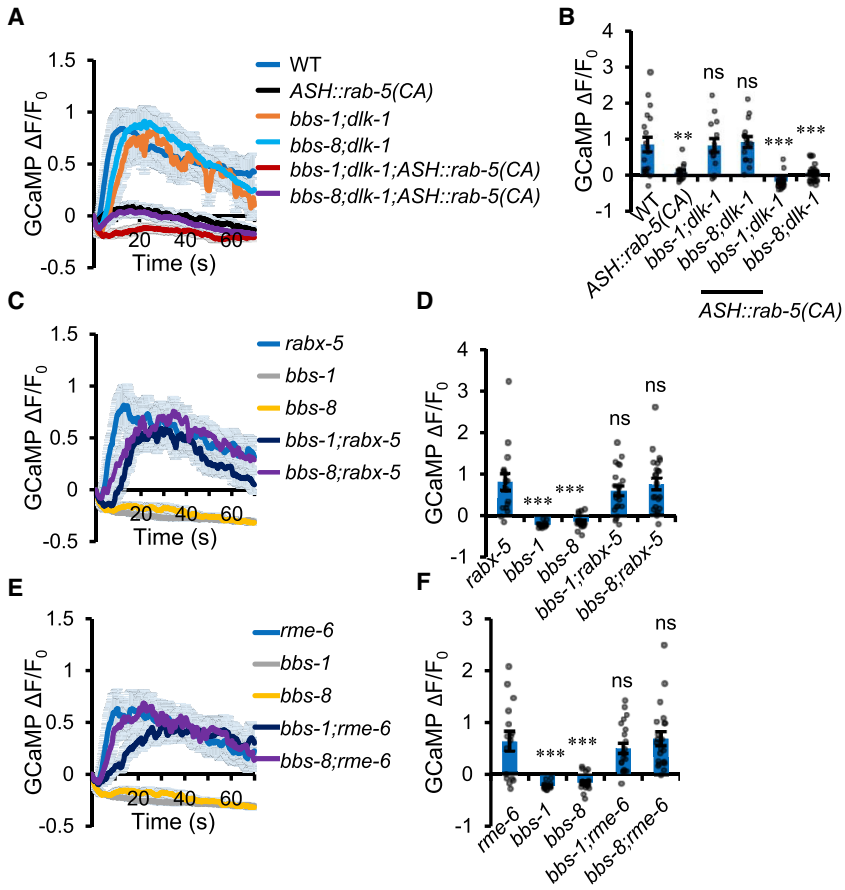

Figure 6. RAB-5 acts downstream of DLK-1/p38MAPK signaling to regulate LITE-1 in ASH neurons

(A and B) Overexpression of RAB-5(CA), a constitutively active form of RAB-5, in ASH neurons strongly suppresses ASH photosensitivity in WT, *bbs-1(ok1111);dlk-1(km12)*, and *bbs-8(nx77);dlk-1(km12)* worms.

(A) Calcium imaging traces. Shades along the traces denote error bars (SEM).

(B) Bar graph. Error bars: SEM; n ≥ 14; **p < 0.005; ***p < 0.0001; ANOVA with Bonferroni test.

(C and D) Loss of the RAB-5 guanine nucleotide exchange factor (GEF) RABX-5 suppresses the photo-insensitivity phenotype of *bbs-1* and *bbs-8* mutant worms. ASH neurons in *bbs-1(ok1111);rabx-5(ok1763)*; and *bbs-8(nx77);rabx-5(ok1763)* double-mutant worms became sensitive to light, while *bbs-1* and *bbs-8* single-mutant worms were not.

(C) Calcium imaging traces. Shades along the traces denote error bars (SEM).

(D) Bar graph. Error bars: SEM; n ≥ 12; **p < 0.005; ***p < 0.0001; ANOVA with Bonferroni test.

(E and F) Loss of the RAB-5 GEF RME-6 suppresses the photo-insensitivity phenotype of *bbs-1* and *bbs-8* mutant worms. ASH neurons in *bbs-1(ok1111);rme-6(b1014)* and *bbs-8(nx77);rme-6(b1014)* double-mutant worms became sensitive to light, while *bbs-1* and *bbs-8* single-mutant worms were not.

(C) Calcium imaging traces. Shades along the traces denote error bars (SEM).

(D) Bar graph. Error bars: SEM; n ≥ 13. ***p < 0.0001; ANOVA with Bonferroni test.

See also Figure S6.

by BBS patients also occurs progressively (Beales et al., 1999). The patients usually begin to lose night vision at an age of ~8.5 years old and become blind when reaching ~15.5 years old (Beales et al., 1999). This phenomenon has also been observed in various mouse models of BBS (Abd-El-Barr et al., 2007; Datta et al., 2015; Nishimura et al., 2004). Specifically, retinal degeneration and signaling protein mislocalization are commonly associated with vision loss in these mouse models. Notably, photoreceptor cells display an age-dependent loss of the photoreceptor protein rhodopsin in a BBS mouse model (Abd-El-Barr et al., 2007), revealing an interesting analogy between worm and mouse BBSome in regulating the stable expression of photoreceptor proteins. Currently, this role of mammalian BBSome has been attributed to its function in cilia. Our results raise the possibility that a cilia-independent function of BBSome might also contribute to the age-dependent vision loss observed in mouse BBS models and perhaps human patients.

DLK is an effector of BBSome

Through a second round of genetic screen, we identified *dlk-1* as a suppressor of *bbs* mutants. Further analysis revealed that BBSome regulates LITE-1 protein stability via DLK/p38MAPK signaling. BBSome is generally believed to function with IFT complexes (Berbari et al., 2008; Jin et al., 2010; Nager et al., 2017; Seo et al., 2009; Tadenev et al., 2011; Ye et al., 2018; Zhang et al., 2013). The identification of *dlk-1* as a BBSome suppressor is rather surprising, as no functional link between BBSome and DLK-MAPK signaling has previously been noted. This highlights the advantage of unbiased genetic screens. Thus, our work not only unveils a cilia-independent function of BBSome, but also identifies an effector (i.e., DLK) for BBSome.

We further showed that BBSome negatively regulates DLK-1 expression. This points to a model in which BBSome regulates LITE-1 stability by inhibiting DLK-MAPK signaling (Figure 7F). In *C. elegans*, DLK-MAPK signaling plays important roles in regulating synaptogenesis, axon growth, axon regeneration, and endocytosis (Jin and Zheng, 2019). Such roles have been reported in other organisms (Jin and Zheng, 2019). We also found that DLK-MAPK signaling regulates LITE-1 instability via Rab5. Rab5 is well known to promote the endocytosis of membrane receptors, which is typically followed by degradation in late endosomes/lysosomes (Yuan and Song, 2020). We suggest that DLK-MAPK signaling may promote LITE-1 instability through a similar mechanism (Figure 7F). Notably, some of the DLK-MAPK signaling components are localized to both within and outside of cilia (van der Vaart et al., 2015). As such, though BBSome can clearly function outside of cilia to regulate LITE-1, we do not rule out the possibility that BBSome may also do so by acting within cilia.

Unlike other types of MAPKKKs that are often activated by receptor signaling in response to external stimuli, DLK/MAPKKKs are usually self-activated by homomultimerization through their leucine zipper domains and autophosphorylation (Jin and Zheng,

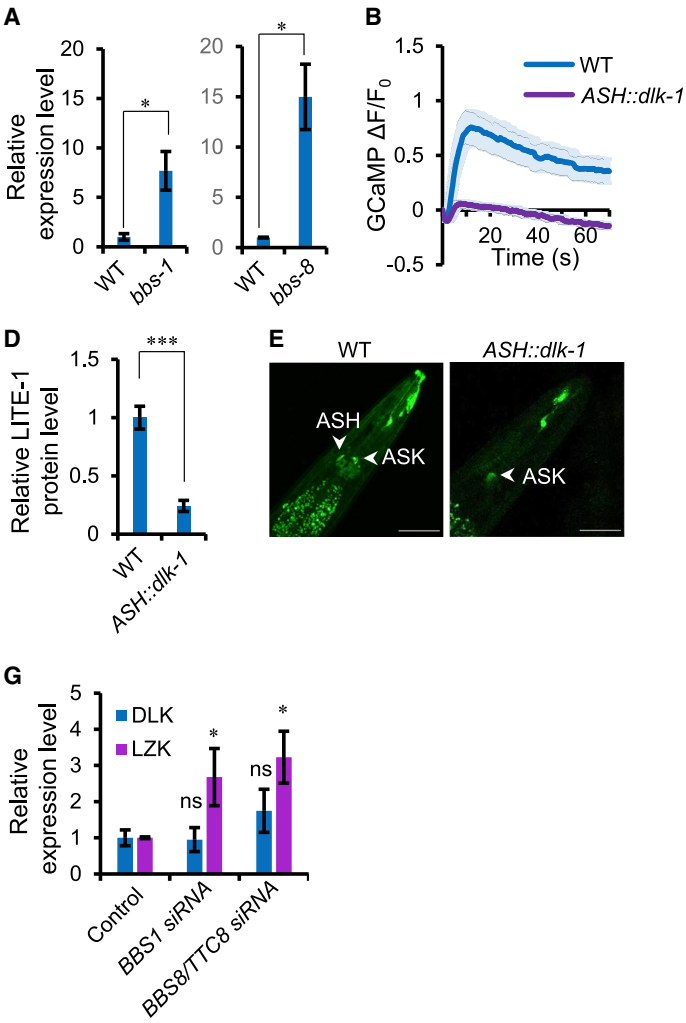

Figure 7. BBSome regulates the expression levels of DLK

(A) *dlk-1* mRNA level in ASH neurons is elevated in *bbs* mutant worms. ASH neurons were purified by FACS. qRT-PCR was performed with RNA extracted from ASH neurons from WT, *bbs-1*, and *bbs-8* worms. Shown are data from three biological replicates, and the experiment was repeated three times. Error bars: SEM; *p < 0.05; t test.

(B and C) Overexpression of DLK-1 in ASH neurons suppress the photosensitivity of ASH neurons. *dlk-1* cDNA was overexpressed in ASH neurons as a transgene using the *sra-6* promoter. The transgene greatly suppressed the photoresponse in ASH neurons.

(B) Calcium imaging traces. Shades along the traces denote error bars (SEM).

(C) Bar graph. Error bars: SEM. Error bars: SEM; n ≥ 18; ***p < 0.0001; t test.

(D and E) Overexpression of DLK-1 in ASH neurons suppresses LITE-1 protein level in ASH neurons. *ASH::dlk-1* transgene was crossed into the *lite-1(xu708[LITE-1::mNeonGreen])* background. The transgene suppressed the LITE-1::mNeon Green fluorescence levels.

(D) Bar graph.

(E) Confocal sample images showing that LITE-1 was not visible in ASH neurons expressing *dlk-1* transgene. Error bars: SEM; n ≥ 23; ***p < 0.0001; t test. Scale bar: 50 μm.

(F) Schematic model showing the genetic pathway underlying BBSome regulation of LITE-1.

(G) BBSome negatively regulates the expression of the human DLK-1 homolog LZK in HeLa cells. Control siRNA or human BBS1 and BBS8/TTC8 siRNA were transfected into HeLa cells. qRT-PCR showed that siRNA knock down of BBS1 and BBS8/TTC8 suppressed the mRNA level of LZK but not DLK, both of which are DLK-1 homologs. Shown are data from three biological replicates, and the experiment was repeated three times. Error bars: SEM. *p < 0.05 (ANOVA with Dunnett test).

See also Figure S7.

2019). This self-activation feature makes the regulation of DLK/MAPKKKs expression levels a key mechanism to modulate DLK/MAPKKK signaling (Jin and Zheng, 2019). Indeed, the conserved E3 ubiquitin ligase RPM-1/Hiw/Phr negatively regulates DLK/MAPKKK protein levels (Jin and Zheng, 2019). Several other proteins have also been proposed to be DLK-1 regulators, including PKA, PPM-2, MIG-2, DLK-1S, and kinesin (Baker et al., 2014; Borgen et al., 2017; Hao et al., 2016; Li et al., 2017; Yan and Jin, 2012). Although we have not identified a role for RPM-1 in regulating LITE-1, it remains possible that these DLK-1 regulators may play a role and may do so in conjunction with BBSome. On the other hand, our observation that BBSome can negatively regulate DLK-1 transcript level indicates that the mRNA level of DLK is also subject to regulation, revealing another important avenue to control DLK/MAPKKK expression and hence its activity. Strikingly, BBSome appears to inhibit the expression of LZK, a mammalian DLK, in human cells. This suggests that regulation of DLK-MAPK signaling by BBSome may be evolutionarily conserved, identifying BBSome as an evolutionarily conserved regulator of DLK.

Limitations of the study

The current study raises many interesting questions. For example, we showed that LITE-1 protein becomes unstable in *bbs* mutants of ASH photosensory neurons; interestingly, this phenomenon is not observed in other photosensory neurons such as ASK. How such a specificity is determined is unclear. It is also unknown why the LITE-1 instability phenotype becomes more severe in adulthood. Lastly, although we found that BBSome regulates DLK-1 by inhibiting its expression, exactly how BBSome does so is currently unknown. Future studies will address these unanswered questions.

STAR★METHODS

Detailed methods are provided in the online version of this paper and include the following:

- KEY RESOURCES TABLE
- RESOURCE AVAILABILITY
  - Lead contact

SUPPLEMENTAL INFORMATION

Supplemental information can be found online at https://doi.org/10.1016/j.devcel.2022.05.005.

ACKNOWLEDGMENTS

We thank Jinhua Hu and Cori Bargmann for strains, Patrick McGrath for CRISPR-Cas9 plasmids, Ken Inoki for providing HeLa cells, and Michel Leroux for critical advice. A.W. was supported by a predoctoral training grant from the NEI (T32EY013934). Some strains were obtained from the Caenorhabditis Genetics Center (CGC) and National BioResource Project (NBRP). This work was supported by the NIGMS (R35GM126917 to X.Z.S.X.).

AUTHOR CONTRIBUTIONS

X.Z. and Jinzhi L. performed the experiments and analyzed the data. X.Z. and T.P. performed the HeLa cell experiment and analyzed the data. A.W. generated critical reagents. X.Z., Jianfeng L., and X.Z.S.X. wrote the paper with assistance from other authors.

DECLARATION OF INTERESTS

The authors declare no competing interests.

Received: May 10, 2021
Revised: April 3, 2022
Accepted: May 4, 2022
Published: May 31, 2022

REFERENCES

Abd-El-Barr, M.M., Sykoudis, K., Andrabi, S., Eichers, E.R., Pennesi, M.E., Tan, P.L., Wilson, J.H., Katsanis, N., Lupski, J.R., and Wu, S.M. (2007). Impaired photoreceptor protein transport and synaptic transmission in a mouse model of Bardet-Biedl syndrome. Vision Res. *47*, 3394–3407.

Ansley, S.J., Badano, J.L., Blacque, O.E., Hill, J., Hoskins, B.E., Leitch, C.C., Kim, J.C., Ross, A.J., Eichers, E.R., Teslovich, T.M., et al. (2003). Basal body dysfunction is a likely cause of pleiotropic Bardet-Biedl syndrome. Nature *425*, 628–633.

Arribere, J.A., Bell, R.T., Fu, B.X., Artiles, K.L., Hartman, P.S., and Fire, A.Z. (2014). Efficient marker-free recovery of custom genetic modifications with CRISPR/Cas9 in Caenorhabditis elegans. Genetics *198*, 837–846.

Bae, Y.K., and Barr, M.M. (2008). Sensory roles of neuronal cilia: cilia development, morphogenesis, and function in C. elegans. Front. Biosci. *13*, 5959–5974.

Baker, S.T., Opperman, K.J., Tulgren, E.D., Turgeon, S.M., Bienvenut, W., and Grill, B. (2014). RPM-1 uses both ubiquitin ligase and phosphatase-based mechanisms to regulate DLK-1 during neuronal development. PLoS Genet. *10*, e1004297.

Bargmann, C.I. (2006). Chemosensation in C. elegans (WormBook), pp. 1–29.

Beales, P.L., Elcioglu, N., Woolf, A.S., Parker, D., and Flinter, F.A. (1999). New criteria for improved diagnosis of Bardet-Biedl syndrome: results of a population survey. J. Med. Genet. *36*, 437–446.

Berbari, N.F., Lewis, J.S., Bishop, G.A., Askwith, C.C., and Mykytyn, K. (2008). Bardet-Biedl syndrome proteins are required for the localization of G protein-coupled receptors to primary cilia. Proc. Natl. Acad. Sci. USA *105*, 4242–4246.

Blacque, O.E., Reardon, M.J., Li, C., McCarthy, J., Mahjoub, M.R., Ansley, S.J., Badano, J.L., Mah, A.K., Beales, P.L., Davidson, W.S., et al. (2004). Loss of C. elegans BBS-7 and BBS-8 protein function results in cilia defects and compromised intraflagellar transport. Genes Dev. *18*, 1630–1642.

Borgen, M.A., Wang, D., and Grill, B. (2017). RPM-1 regulates axon termination by affecting growth cone collapse and microtubule stability. Development *144*, 4658–4672.

Cavalli, V., Vilbois, F., Corti, M., Marcote, M.J., Tamura, K., Karin, M., Arkinstall, S., and Gruenberg, J. (2001). The stress-induced MAP kinase p38 regulates endocytic trafficking via the GDI:Rab5 complex. Mol. Cell *7*, 421–432.

Coburn, C.M., and Bargmann, C.I. (1996). A putative cyclic nucleotide-gated channel is required for sensory development and function in C. elegans. Neuron *17*, 695–706.

Collet, J., Spike, C.A., Lundquist, E.A., Shaw, J.E., and Herman, R.K. (1998). Analysis of osm-6, a gene that affects sensory cilium structure and sensory neuron function in Caenorhabditis elegans. Genetics *148*, 187–200.

Cornils, A., Maurya, A.K., Tereshko, L., Kennedy, J., Brear, A.G., Prahlad, V., Blacque, O.E., and SenGupta, P. (2016). Structural and functional recovery of sensory cilia in C. elegans IFT mutants upon aging. PLoS Genet. *12*, e1006325.

Datta, P., Allamargot, C., Hudson, J.S., Andersen, E.K., Bhattarai, S., Drack, A.V., Sheffield, V.C., and Seo, S. (2015). Accumulation of non-outer segment proteins in the outer segment underlies photoreceptor degeneration in Bardet-Biedl syndrome. Proc. Natl. Acad. Sci. USA *112*, E4400–E4409.

Dickinson, D.J., Pani, A.M., Heppert, J.K., Higgins, C.D., and Goldstein, B. (2015). Streamlined genome engineering with a self-excising drug selection cassette. Genetics *200*, 1035–1049.

Doitsidou, M., Poole, R.J., Sarin, S., Bigelow, H., and Hobert, O. (2010). C. elegans mutant identification with a one-step whole-genome-sequencing and SNP mapping strategy. PLoS One *5*, e15435.

Edwards, S.L., Charlie, N.K., Milfort, M.C., Brown, B.S., Gravlin, C.N., Knecht, J.E., and Miller, K.G. (2008). A novel molecular solution for ultraviolet light detection in Caenorhabditis elegans. PLoS Biol. *6*, e198.

Fan, Y., Esmail, M.A., Ansley, S.J., Blacque, O.E., Boroevich, K., Ross, A.J., Moore, S.J., Badano, J.L., May-Simera, H., Compton, D.S., et al. (2004). Mutations in a member of the Ras superfamily of small GTP-binding proteins causes Bardet-Biedl syndrome. Nat. Genet. *36*, 989–993.

Forsythe, E., Kenny, J., Bacchelli, C., and Beales, P.L. (2018). Managing Bardet-Biedl syndrome-now and in the future. Front. Pediatr. *6*, 23.

Ghanta, K.S., Ishidate, T., and Mello, C.C. (2021). Microinjection for precision genome editing in Caenorhabditis elegans. Star Protoc. *2*, 100748.

Gigante, E.D., Taylor, M.R., Ivanova, A.A., Kahn, R.A., and Caspary, T. (2020). ARL13B regulates Sonic hedgehog signaling from outside primary cilia. eLife *9*.

Gong, J., Liu, J., Ronan, E.A., He, F., Cai, W., Fatima, M., Zhang, W., Lee, H., Li, Z., Kim, G.H., et al. (2019). A cold-sensing receptor encoded by a glutamate receptor gene. Cell *178*, 1375–1386.e11.

Gong, J., Yuan, Y., Ward, A., Kang, L., Zhang, B., Wu, Z., Peng, J., Feng, Z., Liu, J., and Xu, X.Z.S. (2016). The C. elegans taste receptor homolog LITE-1 is a photoreceptor. Cell *167*, 1252–1263.e10.

Hao, Y., Frey, E., Yoon, C., Wong, H., Nestorovski, D., Holzman, L.B., Giger, R.J., DiAntonio, A., and Collins, C. (2016). An evolutionarily conserved mechanism for cAMP elicited axonal regeneration involves direct activation of the dual leucine zipper kinase DLK. eLife *5*, e14048.

Inglis, P.N., Ou, G., Leroux, M.R., and Scholey, J.M. (2007). The sensory cilia of Caenorhabditis elegans (WormBook), pp. 1–22.

Jin, H., White, S.R., Shida, T., Schulz, S., Aguiar, M., Gygi, S.P., Bazan, J.F., and Nachury, M.V. (2010). The conserved Bardet-Biedl syndrome proteins assemble a coat that traffics membrane proteins to cilia. Cell *141*, 1208–1219.

Jin, Y., and Zheng, B. (2019). Multitasking: dual leucine zipper-bearing kinases in neuronal development and stress management. Annu. Rev. Cell Dev. Biol. *35*, 501–521.

Kaletsky, R., Lakhina, V., Arey, R., Williams, A., Landis, J., Ashraf, J., and Murphy, C.T. (2016). The C. elegans adult neuronal IIS/FOXO transcriptome reveals adult phenotype regulators. Nature *529*, 92–96.

Lee, B.H., Liu, J., Wong, D., Srinivasan, S., and Ashrafi, K. (2011). Hyperactive neuroendocrine secretion causes size, feeding, and metabolic defects of C. elegans Bardet-Biedl syndrome mutants. PLoS Biol. *9*, e1001219.

Li, J., Zhang, Y.V., Asghari Adib, E., Stanchev, D.T., Xiong, X., Klinedinst, S., Soppina, P., Jahn, T.R., Hume, R.I., Rasse, T.M., and Collins, C.A. (2017). Restraint of presynaptic protein levels by Wnd/DLK signaling mediates synaptic defects associated with the kinesin-3 motor Unc-104. eLife *6*, e24271.

Li, J.B., Gerdes, J.M., Haycraft, C.J., Fan, Y., Teslovich, T.M., May-Simera, H., Li, H., Blacque, O.E., Li, L., Leitch, C.C., et al. (2004). Comparative genomics identifies a flagellar and basal body proteome that includes the BBS5 human disease gene. Cell *117*, 541–552.

Liu, J., Ward, A., Gao, J., Dong, Y., Nishio, N., Inada, H., Kang, L., Yu, Y., Ma, D., Xu, T., et al. (2010). C. elegans phototransduction requires a G protein–dependent cGMP pathway and a taste receptor homolog. Nat. Neurosci. *13*, 715–722.

Loktev, A.V., Zhang, Q., Beck, J.S., Searby, C.C., Scheetz, T.E., Bazan, J.F., Slusarski, D.C., Sheffield, V.C., Jackson, P.K., and Nachury, M.V. (2008). A BBSome subunit links ciliogenesis, microtubule stability, and acetylation. Dev. Cell *15*, 854–865.

López-Cruz, A., Sordillo, A., Pokala, N., Liu, Q., McGrath, P.T., and Bargmann, C.I. (2019). Parallel multimodal circuits control an innate foraging behavior. Neuron *102*, 407–419.e8.

Mak, H.Y., Nelson, L.S., Basson, M., Johnson, C.D., and Ruvkun, G. (2006). Polygenic control of Caenorhabditis elegans fat storage. Nat. Genet. *38*, 363–368.

Nachury, M.V., Loktev, A.V., Zhang, Q., Westlake, C.J., Peränen, J., Merdes, A., Slusarski, D.C., Scheller, R.H., Bazan, J.F., Sheffield, V.C., and Jackson, P.K. (2007). A core complex of BBS proteins cooperates with the GTPase Rab8 to promote ciliary membrane biogenesis. Cell *129*, 1201–1213.

Nager, A.R., Goldstein, J.S., Herranz-Pérez, V., Portran, D., Ye, F., Garcia-Verdugo, J.M., and Nachury, M.V. (2017). An actin network dispatches ciliary GPCRs into extracellular vesicles to modulate signaling. Cell *168*, 252–263.e14.

Nakata, K., Abrams, B., Grill, B., Goncharov, A., Huang, X., Chisholm, A.D., and Jin, Y. (2005). Regulation of a DLK-1 and p38 MAP kinase pathway by the ubiquitin ligase RPM-1 is required for presynaptic development. Cell *120*, 407–420.

Nishimura, D.Y., Fath, M., Mullins, R.F., Searby, C., Andrews, M., Davis, R., Andorf, J.L., Mykytyn, K., Swiderski, R.E., Yang, B., et al. (2004). Bbs2-null mice have neurosensory deficits, a defect in social dominance, and retinopathy associated with mislocalization of rhodopsin. Proc. Natl. Acad. Sci. USA *101*, 16588–16593.

Novas, R., Cardenas-Rodriguez, M., Irigoín, F., and Badano, J.L. (2015). Bardet-Biedl syndrome: is it only cilia dysfunction? FEBS Lett. *589*, 3479–3491.

Ou, G., Blacque, O.E., Snow, J.J., Leroux, M.R., and Scholey, J.M. (2005). Functional coordination of intraflagellar transport motors. Nature *436*, 583–587.

Park, E.C., Glodowski, D.R., and Rongo, C. (2009). The ubiquitin ligase RPM-1 and the p38 MAPK PMK-3 regulate AMPA receptor trafficking. PLoS One *4*, e4284.

Perkins, L.A., Hedgecock, E.M., Thomson, J.N., and Culotti, J.G. (1986). Mutant sensory cilia in the nematode Caenorhabditis elegans. Dev. Biol. *117*, 456–487.

Richmond, J.E., Davis, W.S., and Jorgensen, E.M. (1999). UNC-13 is required for synaptic vesicle fusion in C. elegans. Nat. Neurosci. *2*, 959–964.

Sann, S.B., Crane, M.M., Lu, H., and Jin, Y. (2012). Rabx-5 regulates RAB-5 early endosomal compartments and synaptic vesicles in C. elegans. PLoS One *7*, e37930.

Sato, M., Sato, K., Fonarev, P., Huang, C.J., Liou, W., and Grant, B.D. (2005). Caenorhabditis elegans RME-6 is a novel regulator of RAB-5 at the clathrin-coated pit. Nat. Cell Biol. *7*, 559–569.

Seo, S., Guo, D.F., Bugge, K., Morgan, D.A., Rahmouni, K., and Sheffield, V.C. (2009). Requirement of Bardet-Biedl syndrome proteins for leptin receptor signaling. Hum. Mol. Genet. *18*, 1323–1331.

Speese, S., Petrie, M., Schuske, K., Ailion, M., Ann, K., Iwasaki, K., Jorgensen, E.M., and Martin, T.F. (2007). UNC-31 (CAPS) is required for dense-core vesicle but not synaptic vesicle exocytosis in Caenorhabditis elegans. J. Neurosci. *27*, 6150–6162.

Tadenev, A.L., Kulaga, H.M., May-Simera, H.L., Kelley, M.W., Katsanis, N., and Reed, R.R. (2011). Loss of Bardet-Biedl syndrome protein-8 (BBS8) perturbs olfactory function, protein localization, and axon targeting. Proc. Natl. Acad. Sci. USA *108*, 10320–10325.

Tan, P.L., Barr, T., Inglis, P.N., Mitsuma, N., Huang, S.M., Garcia-Gonzalez, M.A., Bradley, B.A., Coforio, S., Albrecht, P.J., Watnick, T., et al. (2007). Loss of Bardet Biedl syndrome proteins causes defects in peripheral sensory innervation and function. Proc. Natl. Acad. Sci. USA *104*, 17524–17529.

Torayama, I., Ishihara, T., and Katsura, I. (2007). Caenorhabditis elegans integrates the signals of butanone and food to enhance chemotaxis to butanone. J. Neurosci. *27*, 741–750.

van der Vaart, A., Rademakers, S., and Jansen, G. (2015). DLK-1/p38 MAP kinase signaling controls cilium length by regulating RAB-5 mediated endocytosis in Caenorhabditis elegans. PLoS Genet. *11*, e1005733.

Wang, X., Li, G., Liu, J., Liu, J., and Xu, X.Z. (2016). TMC-1 mediates alkaline sensation in C. elegans through nociceptive neurons. Neuron *91*, 146–154.

Ward, A., Liu, J., Feng, Z., and Xu, X.Z. (2008). Light-sensitive neurons and channels mediate phototaxis in C. elegans. Nat. Neurosci. *11*, 916–922.

Wei, Q., Zhang, Y., Li, Y., Zhang, Q., Ling, K., and Hu, J. (2012). The BBSome controls IFT assembly and turnaround in cilia. Nat. Cell Biol. *14*, 950–957.

Williams, C.L., Mcintyre, J.C., Norris, S.R., Jenkins, P.M., Zhang, L., Pei, Q., Verhey, K., and Martens, J.R. (2014). Direct evidence for BBSome-associated intraflagellar transport reveals distinct properties of native mammalian cilia. Nat. Commun. *5*, 5813.

Xu, Q., Zhang, Y., Wei, Q., Huang, Y., Li, Y., Ling, K., and Hu, J. (2015). BBS4 and BBS5 show functional redundancy in the BBSome to regulate the degradative sorting of ciliary sensory receptors. Sci. Rep. *5*, 11855.

Yan, D., and Jin, Y. (2012). Regulation of DLK-1 kinase activity by calcium-mediated dissociation from an inhibitory isoform. Neuron *76*, 534–548.

Yan, D., Wu, Z., Chisholm, A.D., and Jin, Y. (2009). The DLK-1 kinase promotes mRNA stability and local translation in C. elegans synapses and axon regeneration. Cell *138*, 1005–1018.

Ye, F., Nager, A.R., and Nachury, M.V. (2018). BBSome trains remove activated GPCRs from cilia by enabling passage through the transition zone. J. Cell Biol. *217*, 1847–1868.

Yuan, W., and Song, C. (2020). The emerging role of Rab5 in membrane receptor trafficking and signaling pathways. Biochem. Res. Int. *2020*, 4186308.

Zhang, Q., Nishimura, D., Vogel, T., Shao, J., Swiderski, R., Yin, T., Searby, C., Carter, C.S., Kim, G.H., Bugge, K., et al. (2013). BBS7 is required for BBSome formation and its absence in mice results in Bardet-Biedl syndrome phenotypes and selective abnormalities in membrane protein trafficking. J. Cell Sci. *126*, 2372–2380.

Zhang, W., He, F., Ronan, E.A., Liu, H., Gong, J., Liu, J., and Xu, X.Z.S. (2020). Regulation of photosensation by hydrogen peroxide and antioxidants in C. elegans. PLoS Genet. *16*, e1009257.

STAR★METHODS

KEY RESOURCES TABLE

REAGENT or RESOURCE	SOURCE	IDENTIFIER
Bacterial and virus strains		
E. coli: OP50	CGC	OP50
Chemicals, peptides, and recombinant proteins		
tracrRNA	IDT	Cat# 1072532
S. pyogenes Cas9 3NLS protein	IDT	Cat# 1081058
TRIzol LS	Invitrogen	Cat# 10296010
Tetramisole	Sigma-Aldrich	Cat# T1512
sodium azide	Sigma-Aldrich	Cat# S2002
Critical commercial assays		
RNeasy MinElute Cleanup Kit	Qiagen	Cat# 74204
High-Capacity cDNA Reverse Transcription Kit	Applied Biosystems	Cat# 18418012
SYBR Green	Applied Biosystems	Cat# A25742
Experimental models: Cell lines		
HeLa	ATCC	CCL-2
Experimental models: Organisms/strains		
See Table S1	this study	N/A
Oligonucleotides		
FlexiTube siRNA for human *BBS1*	Qiagen	Cat# GS582
FlexiTube siRNA for human *TTC8*	Qiagen	Cat# GS123016
FlexiTube siRNA for negative control	Qiagen	Cat# 1027281
CRISPR-Cas9 crRNA for making xu832 allele, 2 nmol	IDT	N/A
CRISPR-Cas9 crRNA for making xu845 allele, 2 nmol	IDT	N/A
Recombinant DNA		
Plasmid: Psra-6::FLP(flipase)	This Study	pSX1963
Plasmid: Pgpa-13::FRT2::YFP2	This Study	pSX1962
Plasmid: Psra-6::bbs-1(cDNA)::SL2::mCherry2	This Study	pSX2889
Plasmid: Psra-6::bbs-8(cDNA)::SL2::mCherry2	This Study	pSX2980
Plasmid: Psra-6::mksr-2::tagRFP	This Study	pSX2971
Plasmid: Psra-6::lite-1::mNeonGreen::3xFlag(cDNA)	This Study	pSX2891
Plasmid: Psra-6::dlk-1(cDNA)	This Study	pSX3164
Plasmid: Psra-6::rpm-1(cDNA)	This Study	pSX3346
Plasmid: Psra-6::rab-5(Q78L)	This Study	pSX3244
Plasmid: Psra-6::case12	Xu Lab	pSX2208
Plasmid: Psra-6::mCherry	Xu Lab	pSX102
Software and algorithms		
ImageJ	NIH	https://imagej.nih.gov/ij/
GraphPad Prism	GraphPad	Version 8.0.2
Excel	Microsoft	Microsoft Office 365

RESOURCE AVAILABILITY

Lead contact

Further information and requests for resources and reagents should be directed to and will be fulfilled by the lead contact X.Z. Shawn Xu (shawnxu@umich.edu).

Materials availability

This study has generated plasmids and *C. elegans* strains, which are listed in the Key resources table. These reagents will be made available upon request.

Data and code availability

All data reported in this paper will be shared by the lead contact upon request.

This paper does not report original code. Any additional information required to reanalyze the data reported in this study is available from the lead contact upon request.

EXPERIMENTAL MODEL AND SUBJECT DETAILS

Animals

Worms were fed with standard *E. coli* strain OP50 on NGM agar plates at 20°C. Mutants were verified using PCR-based genotyping and sequencing. The specific genotypes of the strains used this study can be found in Table S1 and the Key resources table. Worms carrying extrachromosomal arrays were generated by injecting plasmid DNA into the hermaphrodite gonad. In all cases, the same extrachromosomal arrays were crossed into WT N2 and different mutant backgrounds for expression analysis and calcium imaging.

Cell lines

HeLa cells were cultured in DMEM medium containing 10% fetal bovine serum (heat inactivated) in a 37°C incubator containing 5% CO2. This cell line was obtained from the ATCC. See the Key resources table for details.

METHOD DETAILS

Genetic screen

bbs-1(xu583), osm-12(xu563), bbs-8(xu607), bbs-8(xu608), and *bbs-9(xu579)* were isolated from a forward genetic screen for mutants with light insensitivity phenotype in ASH neurons. *xuIs556* worms co-expressing *Psra-6::case12* and *Psra-6::SL2::mCherry* were mutagenized with 50 mM EMS. 30-50 F2 worms from each F1 plate (2 F1 per plate) were checked directly under a fluorescence dissecting microscope (Zeiss Discovery) coupled with a SOLA light engine LED light source (Lumencor). F2 worms were examined with 5 mW/mm^2 blue light under 1x lens. Light intensity was measured using an optometer (S471, UDT Instruments) coupled with a sensor head (268LP, UDT Instruments). A total of ~36,000 F2 animals were screened. Animals exhibiting no light response, but with normal-looking soma and dendrites in ASH neurons, were picked, and their progeny was re-examined to confirm the phenotype. Counter-screens were performed using 1 M glycerol. Animals exhibiting normal glycerol responses were kept for further analysis.

Mutant strains were crossed with Hawaii strain CB4856, F2 homozygous mutant worms were pooled, and their genomic DNA was extracted and purified using a NucleoSpin DNA RapidLyse kit (Cat. No. 740100) from MACHERY-NAGEL and subjected to pair-end Illumina whole-genome sequencing (Doitsidou et al., 2010). Unique variants were identified using the MiModD software package via the Variant Allele Frequency (VAF) mapping method (https://mimodd.readthedocs.io/en/latest/#). Protein coding variants were identified using SnpEff version 4.3 (http://snpeff.sourceforge.net) and the WS235 reference genome (http://wormbase.org). We attempted to map all 14 alleles, and successfully got 2 *lite-1* alleles, and 5 *bbs* alleles. However, we failed to identify the causative genes for the other 7 alleles (*xu576*, *xu584*, *xu586, xu593*, *xu597*, *xu611*, and *xu618*), likely due to their relatively weaker phenotype.

The suppressor screen was performed similarly as described above. The photo-insensitive strain *bbs-8(nx77)* V; *xuIs556* was mutagenized with EMS. Mutants suppressing the photo-insensitivity phenotype were picked. The three suppressor mutants *xu734, xu735*, and *xu736*, which exhibited the most penetrate phenotype, were crossed with the parental strain six times. The genomic DNA from mutants and their corresponding light-insensitive siblings was extracted and purified as described above and subjected to pair-end Illumina whole-genome sequencing. The genetic mapping process was similar to that described above, except that the Simple Variant Density (SVD) mapping method was used.

Molecular biology

cDNAs of *bbs-1, bbs-8, mksr-2, dlk-1, rpm-1* and *rab-5* were amplified by RT-PCR from N2 worms and inserted downstream of the *sra-6* promoter. *lite-1::mNeonGreen* cDNA was amplified from *xu708* CRISPR/Cas9 knockin strain by RT-PCR. To visualize the transition zone of ASH neurons, cDNA of *mksr-2* was fused in frame with a TagRFP reporter gene at the N-terminus (Cornils et al., 2016). A variant version of *tax-2* promoter, *Ptax-2Δ* (Coburn and Bargmann, 1996), was used to drive the caspase expression in the neurons mediating phototaxis behaviors other than ASH. The constitutively active form of RAB-5, RAB-5(CA), was made using the Q5 Site-Directed Mutagenesis Kit (NEB) with a Q78L substitution (Sann et al., 2012).

lite-1(xu492) is a deletion allele with a 2701 bp fragment deleted by CRISPR/Cas9-based gene editing using a protocol developed by the Fire lab (Arribere et al., 2014). Specifically, four sgRNAs targeting exon 1 (5'-TTTGAATGTGATGATGGTGG-3', 5'- ATGTTTGAATGTGATGATGG-3'), exon 4 (5'-ACTTTTGGCTCTTACCATGG-3'), and exon 6 (5'-GTAGAACAAGATTGCCAAGG-3') were cloned into the pU6 plasmid and injected together with *Peft3::Cas9* and *dpy-10* sgRNA plasmids, and ssDNA donor for

dpy-10(cn64). Both roller and dumpy F1 worms were singled onto NGM plates, and animals with deletions were selected by single worm PCR. The deletion was verified by Sanger sequencing, and the flanking sequences are: 5'-CGTAAAAAACAACATGCCACCAC-2701bp deletion - GGCGGCCACCTACGCCAGTA -3'. *daf-19(xu786)* and *daf-19(xu789)* are deletion alleles with a 594 bp and 1596 bp deletion, respectively, which were generated in the *daf-12(sa204)* background, using the same CRISPR/Cas9 method described above. The five sgRNAs targeting intron 5 (5'- ATAATAAAATGGGGAGTAGG-3'), intron 5 (5'- ACTCAAAGTGCCAAAAG AGG-3'), intron 5 (5'-GAGATAGAAGACGAAGAAGG-3'), exon 8 (5'-CCAATGCAGCTACCGCAAAG-3'), and exon 9 (5'- CCGTCC ACTCAGTCATACCA-3') were used. The deletion was verified by Sanger sequencing and the flanking sequences of *xu786* are: 5'-CCGACGGCTGGGCACCCGCG- 594 bp deletion -TTTGATTGACATCTACGAAA-3'; the flanking sequences of xu789 are: 5'-CGAATTTCCTGGCATATTAT- 1596 bp deletion - CAAGTATTTGCAACAAGGGC-3'. *lite-1(xu708)* is a knock-in allele with an mNeonGreen::3xFlag tag attached to the C-terminus of *lite-1* locus by the self-excising cassette (SEC) method developed by the Goldstein lab (Dickinson et al., 2015). Four sgRNAs targeting the last exon and 3'-UTR region (5'-TTGCGATATTCTGGAGACTC-3', 5'-TCGTGTGGTTTGCGATATTC-3', 5'-GCTTTTATGTGTGAATCGTG-3', and 5'- AGTGACAGCTGAAGATAAAA-3') near the stop codon were cloned into the pU6 plasmid and injected together with Peft3::Cas9, SEC vector pDD268 with 500-700bp homology arms, and *Pmyo-3::mCherry* marker. Homozygous rollers were selected using hygromycin, and the selectable marker was removed following heat shock. The insertion was confirmed by Sanger sequencing.

bbs-1(xu832[BBS-1::spGFP1-10]) and *dlk-1(xu845[mNeonGreen::dlk-1])* are both knockin alleles made by injecting RNP mixtures as described previously (Ghanta et al., 2021). In brief, repair templates were amplified using unmodified primers with 35 bp homology arms against the target genes from either an spGFP1-10 or mNeongreen plasmid. The RNP mixture was assembled at 37 °C for 15 min and contained Cas9 protein, tracrRNA, and crRNA (all from IDT). crRNA corresponding DNA target sequences are 5'-GAAAACTGGAACTAATCAAG-3' (*bbs-1*), and 5'- TAAAATGACATCTACCACAA-3' (*dlk-1*). The double-strand donor templates were melted right before adding them to the assembled RNPs. Microinjection quality was scored using a co-injection marker, PRF4::*rol-6 (su1006)* plasmid. In general, 10-18 P0 were injected, singled, and maintained at 25 °C for 3 days. Two plates with the highest number of F1 rollers (usually more than 20 rollers for a good injection) were selected, and 24 F1 non-rollers from each plate were picked and singled for further genotyping. The positive insertions were confirmed by Sanger sequencing.

Microscopy

Worms were mounted on 2% agarose pads with 20 mM sodium azide (Sigma-Aldrich, Cat. No. S2002) or tetramisole (Sigma-Aldrich, Cat. No. T1512) in M9 solution. Images were acquired with a Nikon A1 confocal microscope or a Nikon spinning disk confocal with a 60X lens and were processed using ImageJ (NIH). Maximum intensity Z-projection images were shown to illustrate the endogenous LITE-1 protein expression pattern. To quantify the LITE-1 protein expression level, sum slices Z-projection were used. An auto threshold was applied to get the mean intensity of LITE-1::mNeonGreen fluorescence in ASH neurons, which were further corrected by background subtraction. A ratio between the corrected mean intensity of LITE-1::mNeonGreen fluorescence in ASH and background was tabulated for each worm of each genotype, and normalized against that in WT worms to quantify the relative protein expression level of LITE-1. For those ASH neurons that lost LITE-1 expression, the corrected mean intensities were set as zero.

Calcium imaging

Day 1 adult worms were used in all experiments unless noted otherwise. Animals were immobilized using cyanoacrylate adhesive glue to record light response or using microfluidic chips to record chemical responses. All GCaMP signals were recorded with MetaFluor software (Molecular Devices) and a Hamamatsu sCMOS camera (Orca Flash 4.0 LT) using a 40x lens on an Olympus IX73 microscope. Worms carrying a GCaMP6f transgene in ASH neurons and GCaMP5A in ASK neurons were used for calcium imaging (López-Cruz et al., 2019). 20 μL M9 buffer was added to cover the worm glued on a 2% agarose pad. Worms were allowed to rest for 3 min before 5.6 mW/mm2 480 nm blue light stimulus was applied to excite GCaMP and trigger the photoresponse in ASH. Images were acquired at 10 Hz frame rate with 100 ms exposure time. A total of 700 frames were recorded for each worm.

To record ASH responses to 1 M glycerol, 1 mM CuCl2, and 0.1% SDS, worms were immobilized in a microfluidic chip as previously described (Gong et al., 2019; Wang et al., 2016). All chemicals were dissolved in M13 buffer (30 mM Tris-HCl, 100 mM NaCl, 10 mM KCl, pH 7.0). Worms were imaged with 480 nm and 565 nm light simultaneously, and both GCaMP fluorescence and dsRed fluorescence were recorded. Worms were pre-exposed to imaging light for 1-5 min to quench the photoresponse in ASH neurons. After the basal line became stable, a 30 s stimulus pulse was applied to the worm. Each worm was challenged once only with the stimulus. Data were presented as $\Delta R/R0$ ($\Delta R=R-R0$, $R=F_{GCaMP6f}/F_{dsRed}$).

Phototaxis behavior

Phototaxis behavior was analyzed as described previously (Ward et al., 2008). Briefly, day 1 adult worms were transferred to NGM plates covered with a thin layer of freshly spread OP50 bacteria ~30 min before the assay. Worms were tested under a 10x objective on a fluorescence dissection microscope (Zeiss Discovery). A 2 s light pulse (350±25 nm, 406 μW/mm2, Sola, Lumencor) was delivered to the head of a worm that was slowly moving forward. A positive response was scored if the worm stopped forward movement during the illumination time or 3 s after and initiated a backward movement that lasted at least half a head swing.

qRT-PCR analysis

ASH neurons were marked with *xuIs471*[*Pgpa-13*::*FLPase+Psra-6::FRT2::yfp2*] transgene. ASH neurons were isolated from WT, *bbs-1(ok1111)* or *bbs-8(nx77)* adult worms carrying *xuIs471* transgene by fluorescence flow cytometry (FACSAria III cell sorter) using a protocol described previously (Kaletsky et al., 2016). TRIzol LS (Invitrogen, Cat. No. 10296010) was used to extract the total RNA from ASH neurons. RNA samples were further treated with DNaseI (Qiagen, Cat. No. 79254) and cleaned using RNeasy MinElute Cleanup Kit (Qiagen, Cat. No. 74204). High-Capacity cDNA Reverse Transcription Kit (Applied Biosystems, Cat. No. 4368814) was used to synthesize cDNA using oligo dT primer (Invitrogen, Cat. No. 18418012). SYBR Green was used for qPCR analysis (Applied Biosystems, Cat. No. A25742), and samples were run on a QuantStudio™ 5 System (Applied Biosystems, Cat. No. A33628) using a 384-well plate. *act-1* and *pmp-3* were used as housekeeping genes for *lite-1* gene expression analysis. *act-1* forward primer is 5'- CCAGGAATTGCTGATCGTATGCAGAA-3', and the reverse primer is 5'- TGGAGAGGGAAAGCGAGGATAGA-3′. *pmp-3* forward primer is 5′-TGGCCGGATGATGGTGTCGC-3′, and the reverse primer is 5′- ACGAACAATGCCAAAGGCCAGC-3′. *lite-1* forward primer is 5′- TGCTGGCTTCATTGCAACTAT-3′, and the reverse primer is 5′- TTCAACGAAAACTGGCACAA-3′. The experiments were designed to include three biological replicates for each sample and then repeated three times.

HeLa cells were maintained in DMEM media (Gibco, Cat. No.11995065) supplemented with 10% heat-inactivated FBS (Gibco, Cat. No. 10438026) at 37°C under 5% CO2. FlexiTube siRNAs for human *BBS1* (Cat. No. GS582), human *TTC8* (Cat. No. GS123016), and negative control (Cat. No. 1027281) were purchased from Qiagen. Cells were maintained in 35 mm tissue culture dishes (Fisher, Cat. No. FB012920) until 60%-80% confluency, and then transfected with Lipofectamine 2000 reagent (Invitrogen, Cat. No. 11668019) according to manufacturer's instructions with 20 pmol siRNAs for 48 h. RNA extraction, reverse transcription, and qRT-PCR were done as described above. *GAPDH* and *UBC* were used as housekeeping genes. GAPDH forward primer is 5'- TGCACCACCA ACTGCTTAGC-3', and the reverse primer is 5'- GGCATGGACTGTGGTCATGAG-3'. *UBC* forward primer is 5'- ATTTGGGTCG CGGTTCTTG-3', and the reverse primer is 5'- TGCCTTGACATTCTCGATGGT-3'. *DLK* forward primer is 5'- TGCTAATCACCTAC GACGATGT-3', and the reverse primer is 5'- GATCTCACCAGTCAGCAGTTC -3'. *LZK* forward primer is 5'- TGCGCTGGATATTCGT GAACA -3', and the reverse primer is 5'- TCCTTCTCCCGCATTTCTAGC -3'.

QUANTIFICATION AND STATISTICAL ANALYSIS

Statistical analysis was performed in GraphPad Prism.

Developmental Cell, Volume *57*

Supplemental information

A cilia-independent function of BBSome mediated by DLK-MAPK signaling in *C. elegans* photosensation

Xinxing Zhang, Jinzhi Liu, Tong Pan, Alex Ward, Jianfeng Liu, and X.Z. Shawn Xu

Figure S1

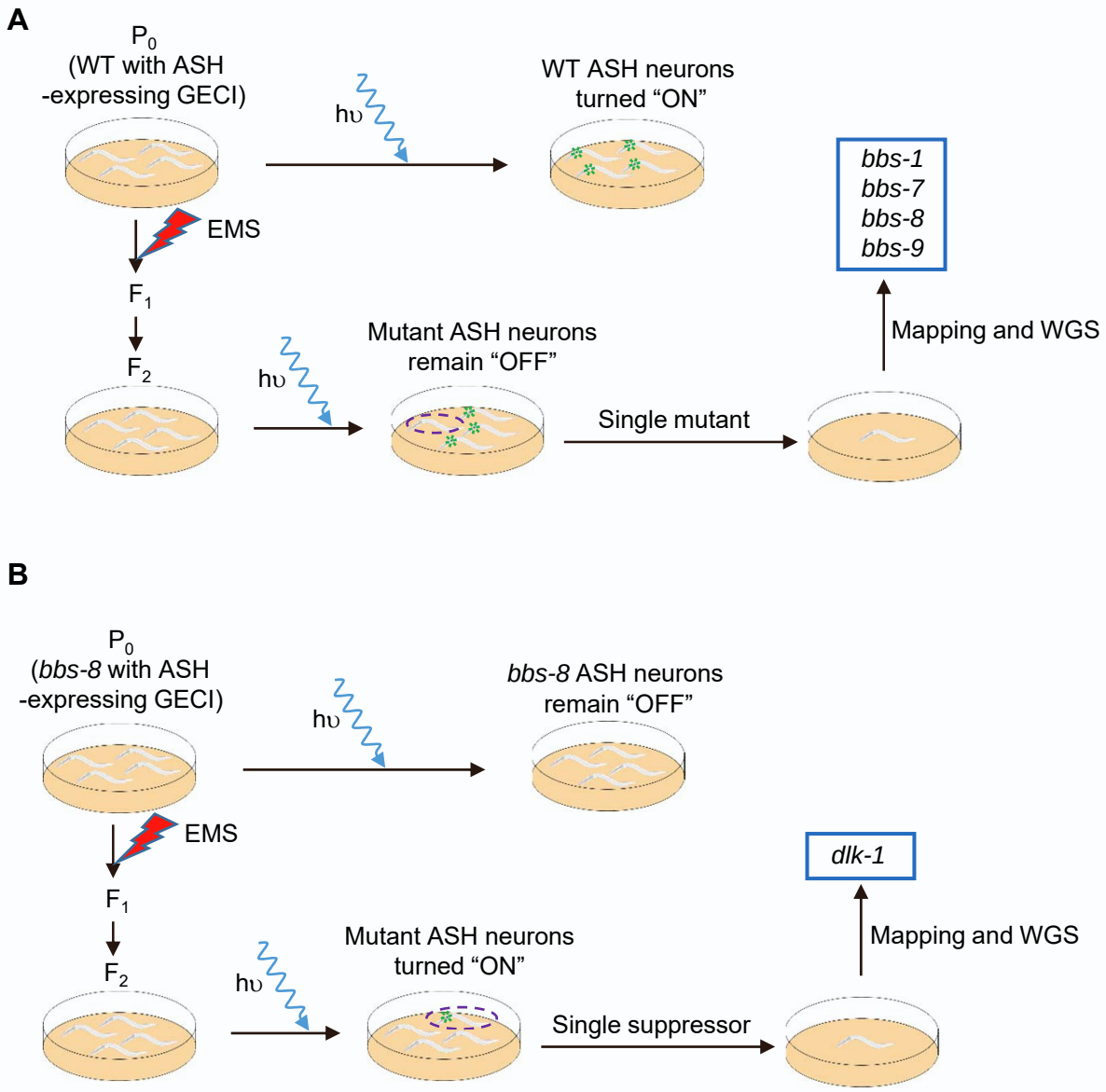

Figure S1. Related to Figure 1 and Figure 4. Schematic diagrams illustrating the genetic screens used to identify *bbs* genes and their downstream effector *dlk-1*. **(A)** A forward genetic screen reveals *bbs* genes regulating the photosensitivity of ASH neurons. **(B)** A suppressor screen uncovers *dlk-1* acting downstream of BBSome.

Figure S2

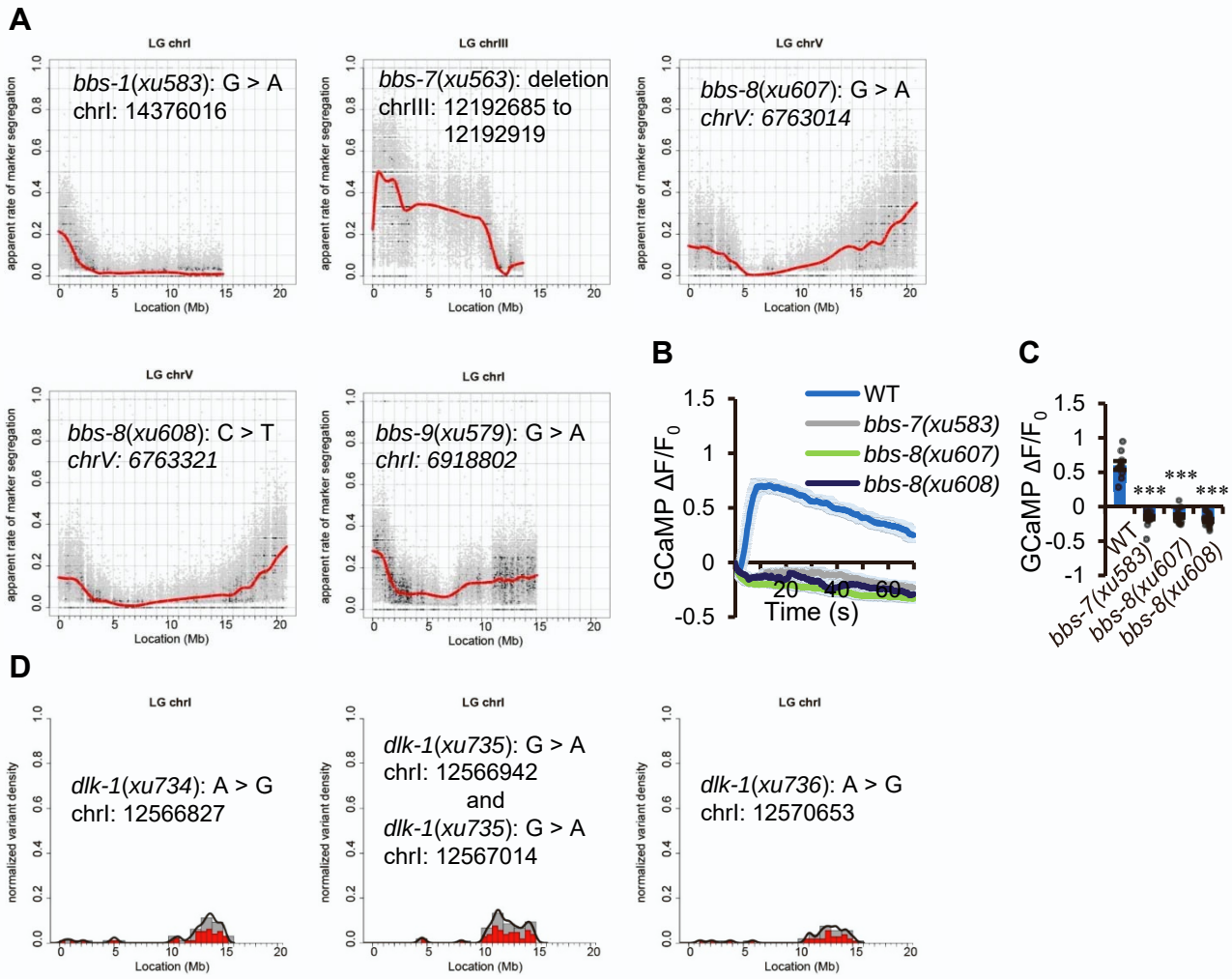

Figure S2. Related to Figure 1 and Figure 4. Mapping plots and locations of mutations in different *bbs* genes and *dlk-1* identified in genetic screens. (A) *bbs* genes were mapped using Hawaiian SNP mapping. **(B-C)** Some *bbs* mutants were further confirmed using calcium imaging, including *bbs-7(xu583), bbs-8(xu607)* and *bbs-8(xu608).* (B) Calcium imaging traces. Shades along the traces denote error bars (SEM). **(C)** Bar graph. Error bars: SEM. n≥10. ***P<0.0001 (ANOVA with Bonferroni test). **(D)** *dlk-1* alleles were mapped using simple variant density (SVD).

Figure S3

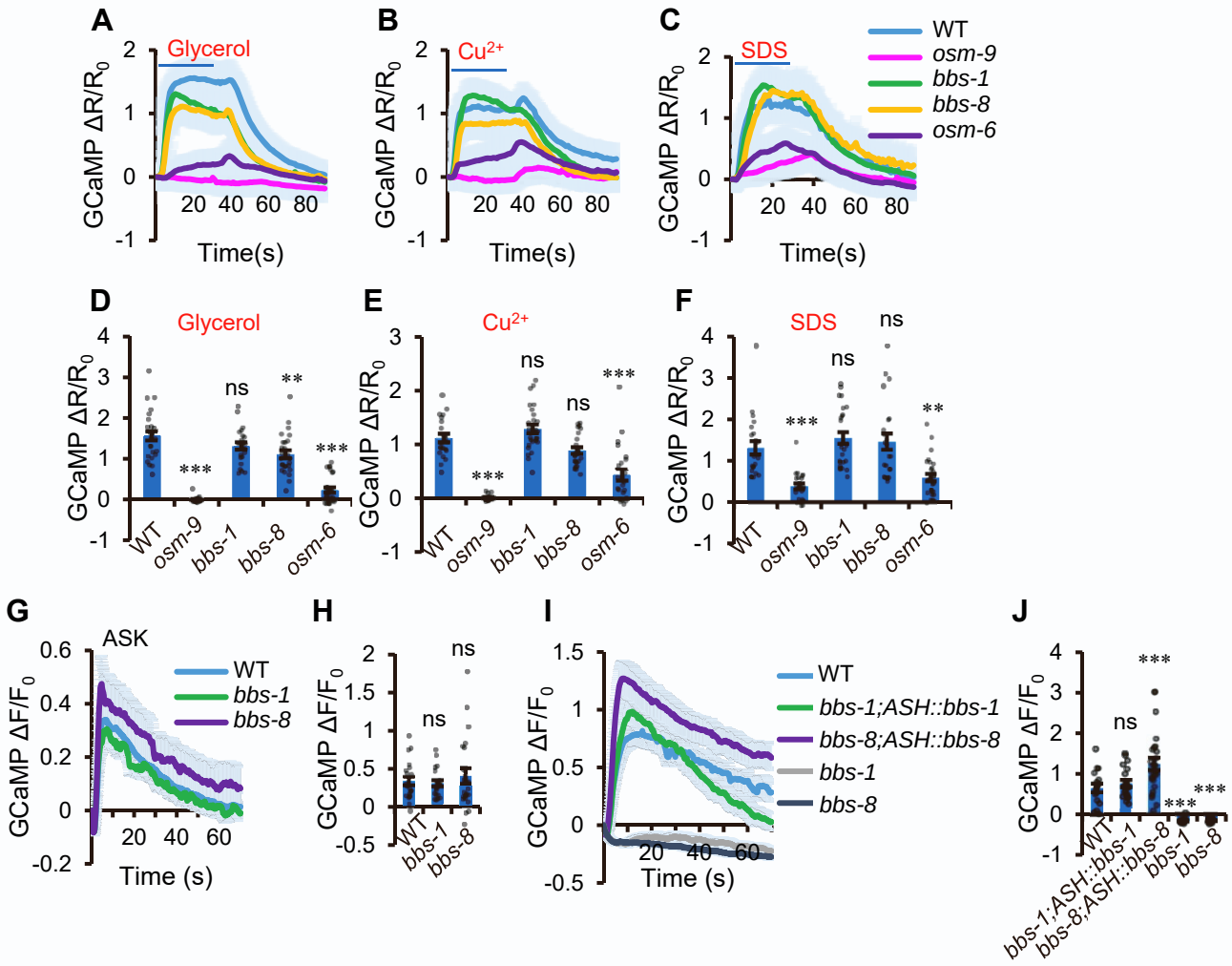
A
Glycerol
GCaMP ΔR/R0
Time(s)
B
Cu2+
C
SDS
WT
osm-9
bbs-1
bbs-8
osm-6
D
E
F
ns
**
***
G
ASK
GCaMP ΔF/F0
Time (s)
H
I
bbs-1;ASH::bbs-1
bbs-8;ASH::bbs-8
J
bbs-1;ASH::bbs-1
bbs-8;ASH::bbs-8

Figure S3. Related to Figure 1. BBSome is specifically required for ASH neurons to sense light.

(A-F) BBSome is not required for ASH neurons to sense aversive cues such as high osmolarity (glycerol), heavy metals (copper), and detergents (SDS). (A-C) ASH neurons in *bbs-1* and *bbs-8* mutant worms respond normally to glycerol (A), copper (B) and SDS (C). All strains carried the same GCaMP transgene. Worms were pre-exposed to blue light to quench the light response to establish a basal line. Subsequently, worms were stimulated by 1 M glycerol, 1 mM Cu^{2+} or 0.1% SDS. *osm-9* and *osm-6* worms were included as controls. Shown are average traces. Shades along the traces denote error bars (SEM). (D-F) Bar graphs summarizing the data in (A-C). Error bars: SEM. Statistics were calculated using One-way ANOVA Bonferroni test, and all strains were compared to wild type. n≥22. *** indicates P<0.0001, ** indicates P<0.005, * indicates P<0.05, and ns indicates not significant.

(G-H) BBSome is not required for ASK neurons to sense light. ASK neurons respond normally to light in *bbs-1(ok1111)* and *bbs-8(nx77)* mutant worms. All worms carried the same GCaMP5A transgene expressed in ASK neurons. (G) Calcium imaging traces. Shades along the traces denote error bars (SEM). (I) Bar graph. Statistics were calculated using One-way ANOVA Bonferroni test, and all strains were compared to wild type. n≥21. ns: not significant.

(I-J) *bbs* genes act in ASH neurons to regulate photosensitivity. The ASH photo-insensitive phenotype of *bbs-1(ok1111)* or *bbs-8(nx77)* mutant worms was rescued by transgenic expression of wild-type *bbs-1* or *bbs-8* cDNA in ASH neurons using the *sra-6* promoter, respectively. (I) Calcium imaging traces. Shades along the traces denote error bars (SEM). (J) Bar graph. n≥21. ns: not significant. ***P<0.0001 (ANOVA with Bonferroni test).

Figure S4

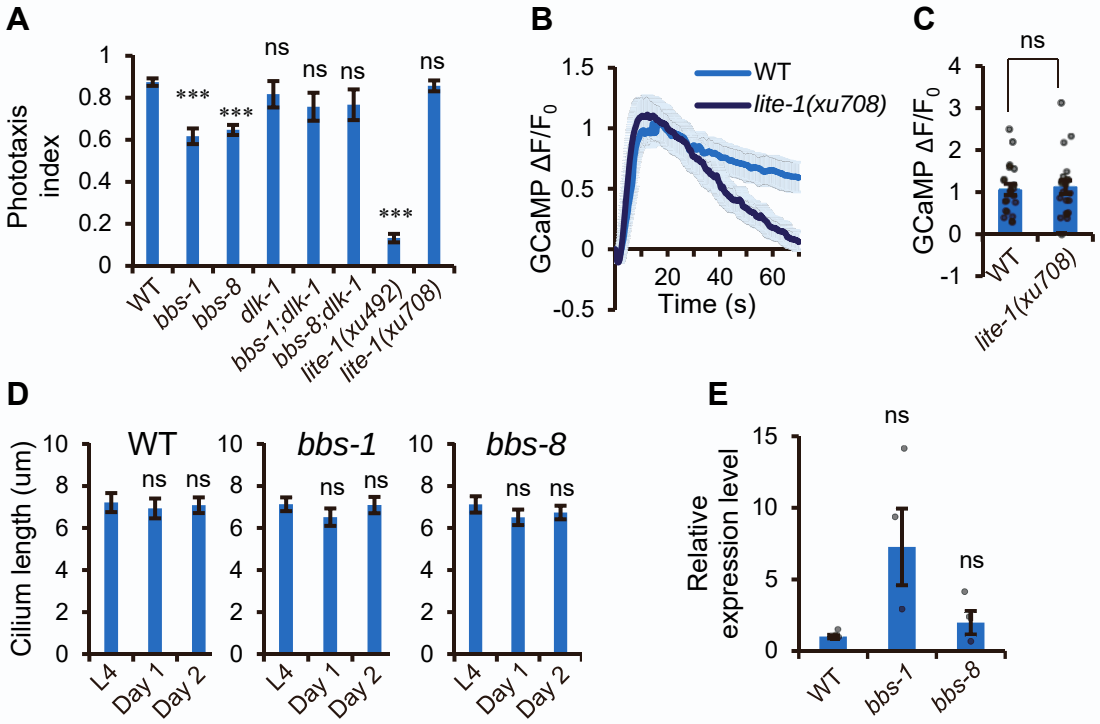
A
Phototaxis index
1
0.8
0.6
0.4
0.2
0
***
***
ns
ns
ns
ns
***
WT
bbs-1
bbs-8
dlk-1
bbs-1;dlk-1
bbs-8;dlk-1
lite-1(xu492)
lite-1(xu708)
B
GCaMP ΔF/F0
1.5
1
0.5
0
-0.5
WT
lite-1(xu708)
20
40
60
Time (s)
C
GCaMP ΔF/F0
4
3
2
1
0
-1
ns
WT
lite-1(xu708)
D
Cilium length (um)
WT
bbs-1
bbs-8
10
8
6
4
2
0
ns
ns
L4
Day 1
Day 2
E
Relative expression level
15
10
5
0
ns
ns
WT
bbs-1
bbs-8

Figure S4. Related to Figure 2 and Figure 3. Additional data related to *bbs* and *lite-1.*

(A) Phototaxis assay shows that *bbs-1(ok1111)* and *bbs-8(nx77)* mutants exhibited a mild defect. This is expected, as BBSome only affects the light sensitivity of ASH neurons but not other photosensory neurons such as ASK. This defect was suppressed by *dlk-1(km12),* as the *bbs;dlk-1* double mutants responded normally. The knock-in allele *lite-1(xu708[LITE-1::mNeonGreen])* showed normal phototaxis behavior, indicating that the mNeonGreen tag fused to the C-terminus of LITE-1 does not affect LITE-1 function. n≥12. Error bars: SEM. ns: not significant. ***P<0.0001 (one-way ANOVA with Bonferroni test).

(B-C) The knock-in allele *lite-1(xu708[LITE-1::mNeonGreen])* responded normally to light in ASH neurons. All strains carried the same GCaMP transgene. (B) Calcium imaging traces. Shades along the traces denote error bars (SEM). (C) Bar graph. n≥21. ns: not significant (t test).

(D) The length of cilia in ASH neurons is normal in *bbs* mutants. Cilium lengths were measured using a diffusible whole-cell marker expressing dsRed in ASH neurons under the *sra-6* promoter in WT, *bbs-1(ok1111)* and *bbs-8(nx77)* worms. There was no statistic difference from L4 to day 2 adults in both WT and *bbs* mutants. ns: not significant (One-way ANOVA with Bonferroni test).

(E) qRT-PCR results show that the *lite-1* mRNA level in ASH neurons is similar between wild type, *bbs-1(ok1111)* and *bbs-8(nx77)* strains. ASH neurons were isolated by fluorescence flow cytometry, and their total RNA were extracted and subjected to qRT-PCR analysis. Shown are data from three biological replicates, and the experiment was repeated three times. Error bars: SEM. Statistics were calculated using One-way ANOVA Bonferroni test, and all strains were compared to wild type. ns: not significant.

Figure S5

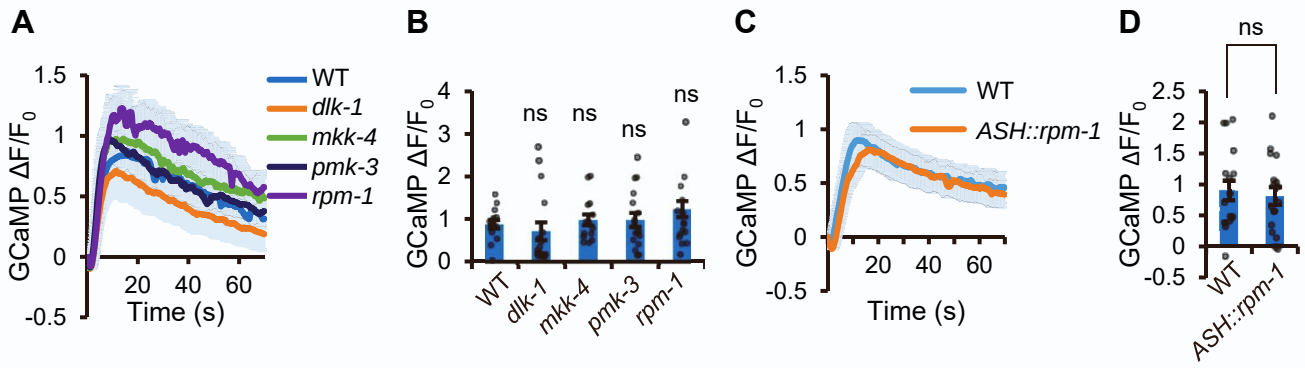

Figure S5. Related to Figure 4 and Figure 5. ASH neurons respond normally to light in *rpm-1, dlk-1*, *mkk-4,* and *pmk-3* mutants, and overexpression of *rpm-1* does not affect ASH photosensitivity.

(A-B) ASH neurons respond normally to light in *rpm-1(ok364)* mutant worms. Although *dlk-1(km12)*, *mkk-4(ok1545)*, *pmk-3(ok169),* and *rpm-1(ok364)* mutants suppressed the phenotype of *bbs* mutant worms, these mutants did not show a notable defect in ASH photosensitivity. (A) Calcium imaging traces. Shades along the traces denote error bars (SEM). (B) Bar graph. Statistics were calculated using One-way ANOVA Bonferroni test, and all strains were compared to WT. n≥15. ns: not significant.

(C-D) Overexpression of *rpm-1* cDNA as a transgene in ASH neurons under the promoter of *sra-6* does not alter the photosensitivity of ASH neurons. (C) Calcium imaging traces. Shades along the traces denote error bars (SEM). (D) Bar graph. n≥17. ns: not significant (t test).

Figure S6

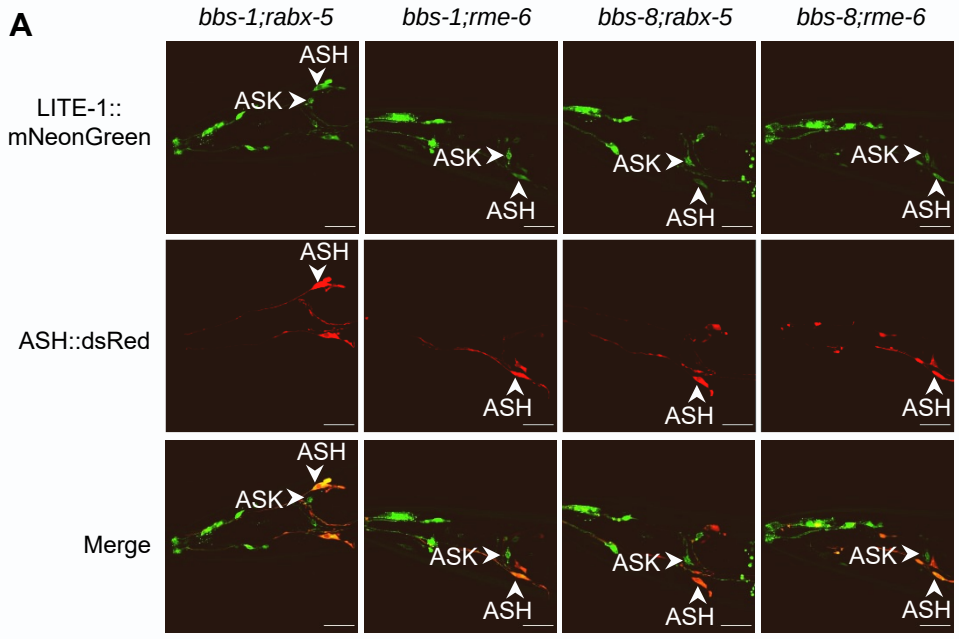

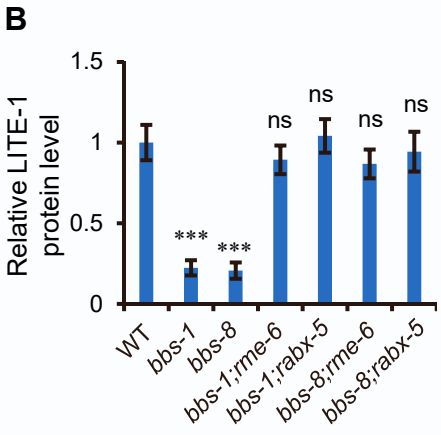

Figure S6. Related to Figure 6. Loss of *rabx-5* and *rme-6* suppresses the LITE-1 instability phenotype in *bbs* mutant worms.

(A) Shown are confocal images for *lite-1(xu708[LITE-1::mNeonGreen]);[Psra-6::dsRed]* in *bbs-1(ok1111);rabx-5(ok1763), bbs-1(ok1111);rme-6(b1014), bbs-8(nx77);rabx-5(ok1763)* and *bbs-8(nx77);rme-6(b1014)* genetic backgrounds at adult (day 2) stage. *lite-1(xu708[LITE-1::mNeonGreen])* is a CRISPR/Cas9 knock-in strain, in which an mNeonGreen tag was fused to the C-terminus of LITE-1. *Psra-6::dsRed* was used to label ASH neurons. Though LITE-1 protein is absent in *bbs-1* and *bbs-8* single mutant adult worms (Figure 3A and 4D), it can now be detected in *bbs;rabx-5* and *bbs;rme-6* double mutants. Scale bar: 20 μm.

(B) Bar graph quantifying LITE-1 protein level. Error bars: SEM. n≥19**.** ns: not significant. ***P<0.0001 (One-way ANOVA with Bonferroni test).

Figure S7

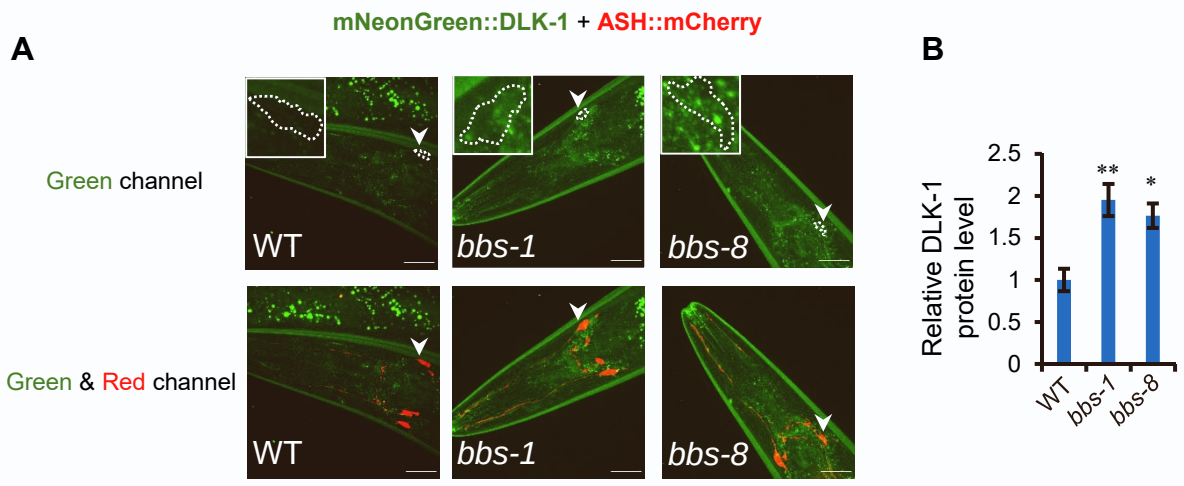

Figure S7. Related to Figure 7. The protein level of endogenous DLK-1 is upregulated in *bbs* mutants.
(A) Shown are confocal images of *dlk-1(xu847[mNeonGreen::DLK-1]);[Psra-6::mCherry]* worms in WT, *bbs-1(ok1111),* and *bbs-8(nx77)* genetic backgrounds at the adult (day 1) stage. *dlk-1(xu847[mNeonGreen::DLK-1])* is a CRISPR knock-in strain, in which an mNeonGreen tag was fused to the N-terminus of DLK-1. The *Psra-6::mCherry* transgene was used to label ASH neurons. Arrows point to ASH neuron soma marked by dotted lines in white. The inset images in the top panel highlight mNeonGreen::DLK-1 fluorescence in ASH soma at a higher magnification. mNeonGreen::DLK-1 fluorescence is mostly visible as puncta structures. Scale bar: 20 μm.
(B) Bar graph quantifying the data in (A). Error bars: SEM. n≥20**.** *P<0.05, **P<0.005 (One-way ANOVA with Bonferroni test).

Supplemental Table S1, related to the STAR Methods and the Key Resources Table, *C. elegans* strains used in this study.

Wild type: N2.	CGC	TQ3030
bbs-1(ok1111) I	CGC	TQ9258
bbs-8(nx77) V	CGC	TQ9255
lite-1(xu492) X	This Study	TQ8029
lite-1(xu708[LITE-1::mNenoGreen::3XFlag]) X	This Study	TQ9387
N2; xuIs556[Psra-6::Case12+Psra-6::SL2::mCherry]	This Study	TQ8866
bbs-1(xu583) I; xuIs556[Psra-6::Case12+Psra-6::SL2::mCherry]	This Study	TQ8979
osm-12(xu563) III; xuIs556[Psra-6::Case12+Psra-6::SL2::mCherry]	This Study	TQ8947
bbs-8(xu607) V; xuIs556[Psra-6::Case12+Psra-6::SL2::mCherry]	This Study	TQ9028
bbs-8(xu608) V; *xuIs556*[*Psra-6::Case12+Psra-6::SL2::mCherry*]	This Study	TQ9030
bbs-9(xu579) I; xuIs556[Psra-6::Case12+Psra-6::SL2::mCherry]	This Study	TQ8972
N2; *xuEx1978*[*Psra-6::GCaMP6f+Psra-6::SL2::DsRed*]	This Study	TQ5856
unc-13(e51) I; *xuEx1978[Psra-6::GCaMP6f+Psra-6::SL2::DsRed]*	This Study	TQ9613
unc-31(e169) IV; *xuEx1978*[*Psra-6::GCaMP6f+Psra-6::SL2::DsRed*]	This Study	TQ9614
lite-1(xu492) X; *xuEx1978*[*Psra-6::GCaMP6f+Psra-6::SL2::DsRed*]	This Study	TQ8220
bbs-1(ok1111) I; *xuEx1978*[*Psra-6::GCaMP6f+Psra-6::SL2::DsRed*]	This Study	TQ9467
bbs-2(ok2053) IV; *xuEx1978*[*Psra-6::GCaMP6f+Psra-6::SL2::DsRed*]	This Study	TQ9465
arl-6/bbs-3(ok3472) III; *xuEx1978*[*Psra-6::GCaMP6f+Psra-6::SL2::DsRed*]	This Study	TQ9474
bbs-4(tm3038) III; *xuEx1978*[*Psra-6::GCaMP6f+Psra-6::SL2::DsRed*]	This Study	TQ9478
bbs-5(gk537) III; *xuEx1978*[*Psra-6::GCaMP6f+Psra-6::SL2::DsRed*]	This Study	TQ9475
osm-12/bbs-7(ok1351) III; *xuEx1978*[*Psra-6::GCaMP6f+Psra-6::SL2::DsRed*]	This Study	TQ9476
bbs-8(nx77) V; *xuEx1978*[*Psra-6::GCaMP6f+Psra-6::SL2::DsRed*]	This Study	TQ9468
bbs-9(gk471) I; *xuEx1978*[*Psra-6::GCaMP6f+Psra-6::SL2::DsRed*]	This Study	TQ9473
che-3(e1124) I; *xuEx1978*[*Psra-6::GCaMP6f+Psra-6::SL2::DsRed*]	This Study	TQ9636
osm-3(p802) IV; *xuEx1978*[*Psra-6::GCaMP6f+Psra-6::SL2::DsRed*]	This Study	TQ7538
kap-1(ok676) II; *xuEx1978*[*Psra-6::GCaMP6f+Psra-6::SL2::DsRed*]	This Study	TQ9479
klp-11(tm324) IV; *xuEx1978*[*Psra-6::GCaMP6f+Psra-6::SL2::DsRed*]	This Study	TQ9634
daf-10(e1387) IV; *xuEx1978*[*Psra-6::GCaMP6f+Psra-6::SL2::DsRed*]	This Study	TQ9737
osm-5(p813) X; xuEx1978[Psra-6::GCaMP6f+Psra-6::SL2::DsRed]	This Study	TQ9639
osm-6(p811) V; *xuEx1978*[*Psra-6::GCaMP6f+Psra-6::SL2::DsRed*]	This Study	TQ9749
bbs-1(ok1111) I; *xuEX3284[Psra-6::bbs-1(cDNA)::sl2::m2+Punc122::gfp]; xuEx1978*[*Psra-6::GCaMP6f+Psra-6::SL2::DsRed*]	This Study	TQ9715
bbs-8(nx77) V; *xuEX3286[Psra-6::bbs-8(cDNA)::sl2::m2+Punc122::gfp]; xuEx1978*[*Psra-6::GCaMP6f+Psra-6::SL2::DsRed*]	This Study	TQ9717
bbs-7(xu563) III; *xuEx1978*[*Psra-6::GCaMP6f+Psra-6::SL2::DsRed*]	This Study	TQ10727
bbs-8(xu607) V; *xuEx1978*[*Psra-6::GCaMP6f+Psra-6::SL2::DsRed*]	This Study	TQ10728
bbs-8(xu608) V; *xuEx1978*[*Psra-6::GCaMP6f+Psra-6::SL2::DsRed*]	This Study	TQ10729
bbs-1(ok1111) I; xuEx3748[Ptax-2Δ::caspase + Punc-122::gfp]	This Study	TQ10916
bbs-8(nx77) V; xuEx3748[Ptax-2Δ::caspase + Punc-122::gfp]	This Study	TQ10917
bbs-1(xu832[BBS-1::spGFP1-10]) I; *xuEx3709[Psra-6::7xspGFP11+Punc-122::gfp]*	This Study	TQ10872
bbs-1(xu832[BBS-1::spGFP1-10]) I; *dyf-2(jhu616*) III; *xuEx3709[Psra-6::7xspGFP11+Punc-122::gfp]; xuEx3749[Psra-6::mcherry+Punc-122::rfp]*	This Study	TQ11051
dyf-2(jhu616) III; *xuEx1978*[*Psra-6::GCaMP6f+Psra-6::SL2::DsRed*]	This Study	TQ10867

daf-19(m86) II; *daf-12(sa204)* X; *xuEx1978*[*Psra-6::GCaMP6f+Psra-6::SL2::DsRed*]	This Study	TQ9629
daf-19(xu786) II; *daf-12(sa204)* X; *xuEx1978*[*Psra-6::GCaMP6f+Psra-6::SL2::DsRed*]	This Study	TQ10222
daf-19(xu789) II; *daf-12(sa204)* X; *xuEx1978*[*Psra-6::GCaMP6f+Psra-6::SL2::DsRed*]	This Study	TQ10227
N2; *xuEx3318*[*Psra-6::lite-1::mNG::3xFlag(cDNA)+Psra-6::mCherry*]	This Study	TQ9827
N2; *xuEx3341*[*Psra-6::lite-1::mNG::3xFlag(cDNA)+Psra-6::mksr-2(cDNA)::TagRFP*]	This Study	TQ9890
osm-9(ok1677) IV; *xuEx1978*[*Psra-6::GCaMP6f+Psra-6::SL2::DsRed*]	This Study	TQ7635
lite-1(*xu708*[LITE-1::mNenoGreen::3XFlag]) X; *xuEx331[Psra-6::dsRed]*	This Study	TQ9477
bbs-1(ok1111) I; *lite-1*(*xu708*[LITE-1::mNenoGreen::3XFlag]) X; *xuEx331[Psra-6::dsRed]*	This Study	TQ9702
bbs-8(nx77) V; *lite-1*(*xu708*[LITE-1::mNenoGreen::3XFlag]) X; *xuEx331[Psra-6::dsRed]*	This Study	TQ9700
bbs-1(ok1111) I; *dlk-1 (km12)* I*; lite-1*(*xu708*[LITE-1::mNenoGreen::3XFlag]) X; *xuEx331[Psra-6::dsRed]*	This Study	TQ10380
bbs-8(nx77) V; *dlk-1 (km12)* I*; lite-1*(*xu708*[LITE-1::mNenoGreen::3XFlag]) X; *xuEx331[Psra-6::dsRed]*	This Study	TQ10381
N2; *kyEx6191*[*Psra-9::GCaMP5A+Pelt-2::mCherry*]	(Lopez-Cruz et al., 2019)	TQ9748
bbs-1(ok1111) I; *kyEx6191*[*Psra-9::GCaMP5A+Pelt-2::mCherry*]	This Study	TQ9618
bbs-8(nx77) V; *kyEx6191*[*Psra-9::GCaMP5A+Pelt-2::mCherry*]	This Study	TQ9619
N2; xuIs471[*Pgpa-13::FLP*ase+*Psra-6::FRT2::yfp2*]	This Study	TQ7810
bbs-1(ok1111) I; xuIs471[*Pgpa-13::FLP*ase+*Psra-6::FRT2::yfp2*]	This Study	TQ9746
bbs-8(nx77) V; xuIs471[*Pgpa-13::FLP*ase+*Psra-6::FRT2::yfp2*]	This Study	TQ9757
bbs-8(nx77) V; *xuIs556*[*Psra-6::Case12+Psra-6::SL2::mCherry*]	This Study	TQ9396
rpm-1(*ok364*) V; *xuEx1978*[*Psra-6::GCaMP6f+Psra-6::SL2::DsRed*]	This Study	TQ10228
dlk-1(*km12*) I; *xuEx1978*[*Psra-6::GCaMP6f+Psra-6::SL2::DsRed*]	This Study	TQ10229
mkk-4(*ok1545*) X; *xuEx1978*[*Psra-6::GCaMP6f+Psra-6::SL2::DsRed*]	This Study	TQ10230
pmk-3(*ok169*) IV; *xuEx1978*[*Psra-6::GCaMP6f+Psra-6::SL2::DsRed*]	This Study	TQ7172
bbs-1(ok1111) I; *dlk-1*(*km12*) I; *xuEx1978*[*Psra-6::GCaMP6f+Psra-6::SL2::DsRed*]	This Study	TQ10274
bbs-8(nx77) V; *dlk-1*(*km12*) I; *xuEx1978*[*Psra-6::GCaMP6f+Psra-6::SL2::DsRed*]	This Study	TQ10235
bbs-1(ok1111) I; *dlk-1*(*km12*) I; *xuEx3559[Psra-6::dlk-1(cDNA)+Punc-122::gfp]; xuEx1978*[*Psra-6::GCaMP6f+Psra-6::SL2::DsRed*]	This Study	TQ10682
bbs-8(nx77) V; *dlk-1*(*km12*) I; *xuEx3559[Psra-6::dlk-1(cDNA)+Punc-122::gfp]; xuEx1978*[*Psra-6::GCaMP6f+Psra-6::SL2::DsRed*]	This Study	TQ10683
bbs-1(ok1111) I; *mkk-4*(*ok1545*) X; *xuEx1978*[*Psra-6::GCaMP6f+Psra-6::SL2::DsRed*]	This Study	TQ10268
bbs-8(nx77) V; *mkk-4*(*ok1545*) X; *xuEx1978*[*Psra-6::GCaMP6f+Psra-6::SL2::DsRed*]	This Study	TQ10237
bbs-1(ok1111) I; *pmk-3*(*ok169*) IV; *xuEx1978*[*Psra-6::GCaMP6f+Psra-6::SL2::DsRed*]	This Study	TQ10270
bbs-8(nx77) V; *pmk-3*(*ok169*) IV; *xuEx1978*[*Psra-6::GCaMP6f+Psra-6::SL2::DsRed*]	This Study	TQ10276
N2; xuEx3705[Psra-6::rab-5(CA)+Punc-122::gfp]; xuEx1978[Psra-6::GCaMP6f+Psra-6::SL2::DsRed]	This Study	TQ10680

bbs-1(ok1111) I; *dlk-1*(*km12*) I; *xuEx3705[Psra-6::rab-5(CA)+Punc-122::gfp]; xuEx1978*[*Psra-6::GCaMP6f+Psra-6::SL2::DsRed*]	This Study	TQ10718
bbs-8(nx77) V; *dlk-1*(*km12*) I; *xuEx3705[Psra-6::rab-5(CA)+Punc-122::gfp]; xuEx1978*[*Psra-6::GCaMP6f+Psra-6::SL2::DsRed*]	This Study	TQ10719
rabx-5(ok1763) III; *xuEx1978*[*Psra-6::GCaMP6f+Psra-6::SL2::DsRed*]	This Study	TQ10687
bbs-1(ok1111) I; *rabx-5(ok1763)* III; *xuEx1978*[*Psra-6::GCaMP6f+Psra-6::SL2::DsRed]*	This Study	TQ10692
bbs-8(nx77) V; *rabx-5(ok1763)* III; *xuEx1978*[*Psra-6::GCaMP6f+Psra-6::SL2::DsRed*]	This Study	TQ10693
rme-6(b1014) X; *xuEx1978*[*Psra-6::GCaMP6f+Psra-6::SL2::DsRed*]	This Study	TQ10686
bbs-1(ok1111) I; *rme-6(b1014)* X; *xuEx1978*[*Psra-6::GCaMP6f+Psra-6::SL2::DsRed]*	This Study	TQ10699
bbs-8(nx77) V; *rme-6(b1014)* X; *xuEx1978*[*Psra-6::GCaMP6f+Psra-6::SL2::DsRed*]	This Study	TQ10691
bbs-1(ok1111) I; *rabx-5(ok1763)* III; *lite-1*(*xu708*[LITE-1::mNenoGreen::3XFlag]) X; *xuEx331[Psra-6::dsRed]*	This Study	TQ10730
bbs-8(nx77) V; *rabx-5(ok1763)* III; *lite-1*(*xu708*[LITE-1::mNenoGreen::3XFlag]) X; *xuEx331[Psra-6::dsRed]*	This Study	TQ10720
bbs-1(ok1111) I; *rme-6(b1014)* X; *lite-1*(*xu708*[LITE-1::mNenoGreen::3XFlag]) X; *xuEx331[Psra-6::dsRed]*	This Study	TQ10731
bbs-8(nx77) V; *rme-6(b1014)* X; *lite-1*(*xu708*[LITE-1::mNenoGreen::3XFlag]) X; *xuEx331[Psra-6::dsRed]*	This Study	TQ10721
bbs-1(ok1111) I; *xuEx331[Psra-6::dsRed]*	This Study	TQ10660
bbs-8(nx77) V; *xuEx331[Psra-6::dsRed]*	This Study	TQ10662
N2; *xuEx3746[Psra-6::rpm-1(cDNA)+Punc-122::gfp]; xuEx1978*[*Psra-6::GCaMP6f+Psra-6::SL2::DsRed*]	This Study	TQ10910
N2; *xuEx3559[Psra-6::dlk-1(cDNA)+Punc-122::gfp]*; *xuEx1978*[*Psra-6::GCaMP6f+Psra-6::SL2::DsRed*]	This Study	TQ10498
lite-1(*xu708*[LITE-1::mNenoGreen::3XFlag]) X; *xuEx3559[Psra-6::dlk-1(cDNA)+Punc-122::gfp]*	This Study	TQ10538
dlk-1(xu845[mNenoGreen::DLK-1]) I*; xuEx3749[Psra-6::mcherry+Punc-122::rfp]*	This Study	TQ11032
bbs-1(ok1111) I; *dlk-1(xu845[mNenoGreen::DLK-1])* I*; xuEx3749[Psra-6::mcherry+Punc-122::rfp]*	This Study	TQ11033
bbs-8(nx77) V; *dlk-1(xu845[mNenoGreen::DLK-1])* I*; xuEx3749[Psra-6::mcherry+Punc-122::rfp]*	This Study	TQ11034